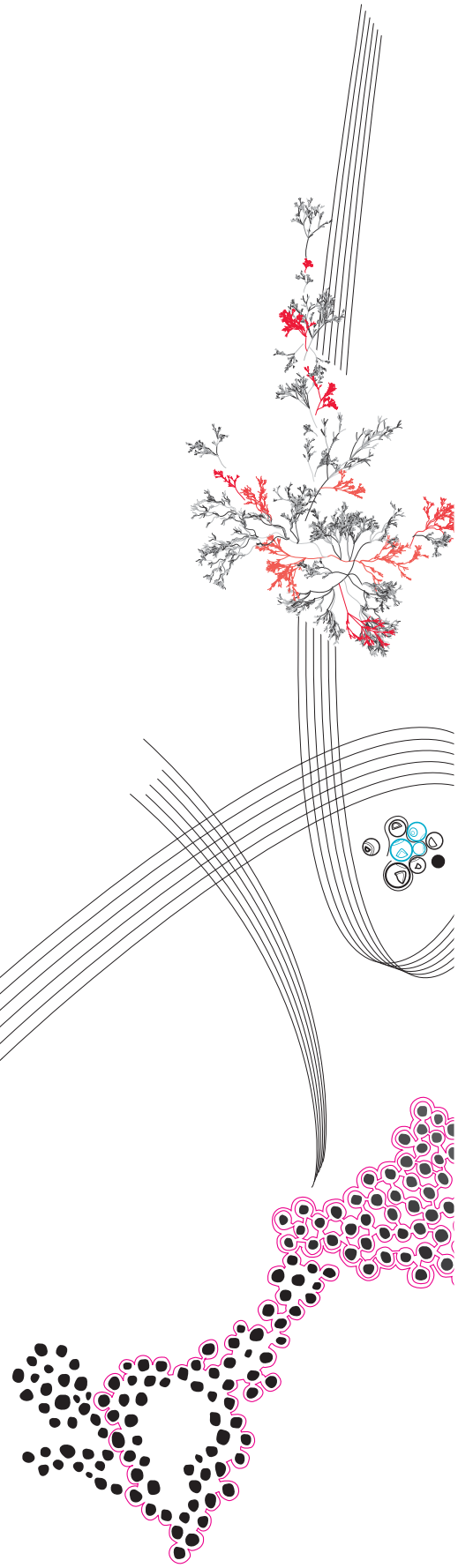

BSc Thesis Applied Mathematics
and Applied Physics

Finding eigenmodes of linear systems using a universal preconditioner with applications to dielectric cavities

Gernt Hanskamp

Supervisors:
Carlos Pérez Arancibia
Ivo Vellekoop

June, 2023

Department of Applied Mathematics
Faculty of Electrical Engineering,
Mathematics and Computer Science

Department of Applied Physics
Faculty of Science and Technology

UNIVERSITY OF TWENTE.

Preface

I started this thesis with almost no knowledge about eigenmodes, let alone quasi-normal modes, and preconditioning. During the project, I have encountered many different methods related to these topics and got a grasp on the main topics. I want to thank a few people who helped me to understand these topics and finish this thesis.

First, I want to thank Carlos Pérez Arancibia for his optimistic views and clear explanations of the difficult subjects I encountered. On top of that, I thank him for his extensive and quick work on giving feedback on draft versions of the report. I want to thank Ivo Vellekoop for his useful feedback and explanations of the preconditioner and the working of the AnySim solver. In addition, I thank Swapnil Mache for his explanation of the code structure of AnySim.

Besides this, I thank my friends to keep me motivated in times I got stuck. Also, I thank them for making me explain the topic in understandable words and trying to understand what I was doing. This helped me to grasp the essential part of my research and think about applications.

Finding eigenmodes of linear systems using a universal preconditioner with applications to dielectric cavities

Gernt Hanskamp

June, 2023

Abstract

A method is introduced that finds eigenmodes of linear systems. These eigenmodes may possibly be quasi-normal modes, where the frequency is complex to model the damping of energy in an open cavity. The method locates eigenfrequencies using the fact that the operator $A(\omega)$ is singular at an eigenfrequency ω_0 and therefore the norm $\|A^{-1}(\omega)\psi\|$ is large for ω close to ω_0, where ψ is a random vector. Thus, the function $f(\omega) = \frac{1}{\|A^{-1}(\omega)\psi\|}$ has a minimum at ω_0. $A^{-1}\psi$ is found by solving the linear system $A\phi = \psi$ using a universal preconditioner and the BiCGSTAB algorithm. The method is validated and illustrated using the Helmholtz equation, applied on a one-dimensional Fabry-Perot resonator and a dielectric circular cavity in two dimensions and compared with analytical solutions. It is found that it locates eigenfrequencies accurately and approximates the eigenfunction well in most cases, except for low-frequency asymmetric modes. Furthermore, the method is illustrated for a distorted circular cavity.

Keywords: eigenmodes, quasi-normal modes, preconditioner

Contents

1 Introduction

Significant effort is put into finding solutions of linear systems. Those linear systems can generally be defined as

$$A\phi = \psi. \tag{1.1}$$

Here A is a linear operator, which can for example be a matrix, a differential operator, or an integral operator. Generally, ψ is given and A is invertible, and the problem is to find ϕ efficiently.

Finding those solutions efficiently is difficult in many situations where the resulting discretized systems are large or ill-conditioned, meaning many iterative methods do not converge or converge slowly. In these cases, one might use a preconditioner to make the system much better conditioned. This preconditioner is essentially an operator which is applied on the entire system (1.1). Recently, a universal preconditioner was constructed by Vettenburg and Vellekoop in [20] that ensures the convergence of many linear systems when using the Richardson iteration method, which is a very simple iteration method.

A different problem related to linear systems is finding the eigenmodes of an operator. In wave equations, such eigenmodes often form a basis for all possible wave functions in the system and show resonating behavior when the system is excited at an eigenfrequency, that gives rise to an eigenmode. Therefore, knowing the eigenmodes can give us a lot of information about the behavior of the system.

For open cavities, quasi-normal modes are used to form a basis for the wave functions inside the cavity. These quasi-normal modes have a complex frequency. The construction of such quasi-normal modes will be explained in Section 2.

We will now describe some applications of eigenmodes in optics.

In optics, there are many applications of optical cavities in an otherwise uniform medium. The resonances determine the scattering of such a cavity since the transmittance and reflectance are determined by how the incoming wave behaves inside the cavity. Therefore, cavities or nanoparticles can be used to isolate or filter out certain frequencies, by using cavities that resonate at the wanted frequency. Also, the analysis of the scattering behavior can be done by using an eigenmode expansion.

Also in medicine, there are many applications of resonating nanoparticles. For example, in [9] it is described how magnetic nanoparticles can be used to destroy cancer cells, where the nanoparticles are designed to accumulate around cancer cells and heat up when excited with a magnetic field that oscillates with the resonating frequency. This method is called magnetic hypothermia. Also in MRI, nanoparticles with specific eigenmodes are used to increase contrast or highlight specific tissues of interest.

Laser technology also relies heavily on determining the resonating behavior of eigenmodes (see e.g. [19]). By achieving resonance, lasers can efficiently generate and amplify coherent light. The eigenmodes can be tuned to change the wavelength or beam shape of the laser.

In this thesis, we will construct a method that efficiently finds eigenfrequencies and approximates eigenfunctions for time-harmonic solutions to wave equations. The method uses the preconditioner mentioned above.

Finding such eigenmodes of an operator is often computationally expensive, as some methods involve inverting the operator many times, for example when using Arnoldi's

method, introduced in [3]. Therefore, using a good preconditioner will improve the efficiency of such methods. Other methods only find a subset of the eigenvalues, like the power iteration that only finds the eigenvalue with largest absolute value.

Another method that is often used to find eigenmodes is the finite element method. This method uses linear algebra methods after discretizing the system. Different iterative methods to find eigenvalues of a matrix exist, but generally are not efficient, because the discretized system consists of full matrices that are inefficient to do operations on. Our method using the preconditioner is very efficient, because the preconditioned operator uses the Fast Fourier Transform when solving the system. Furthermore, [8] showed that the finite element method is not accurate for wave guide problems and time-harmonic wave solutions with high frequency, making it not universally applicable.

To adress these shortcomings, we will introduce another approach, which is able to find all eigenfrequencies of the eigenmodes inside a finite frequency domain. Here solutions to the linear system are computed for different frequencies. A random source ψ is applied and the preconditioner is used to find solutions to the linear system $A(\omega)\phi = \psi$.

The random source will excite the eigenmodes, if present, and the amplitude of the resonant field ϕ will be large inside the cavity when the frequency is close to a resonating frequency. This fact is used to construct a method that locates the modes, which comes down to find the frequency that minimizes $\frac{1}{\|\phi\|}$. A formalized description of the method is given in Section 4.

Validations of our method will be done in Section 5 by comparing the numerical results to analytical solutions of relatively simple systems for which the analytical solution can be found. These are a Fabry-Perot resonator in one dimension in Section 5.1 and a dielectric circular cavity in two dimensions in Section 5.2. We will also illustrate that our method yields useful results for other shapes in Section 5.3, namely a slightly distorted dielectric circular cavity, in which the circular symmetry is removed.

The method we will introduce will be valid for time-harmonic solutions to wave equations. For simplicity, however, we decide to use the Helmholtz equation to validate our method. This equation follows from the wave equation for the electric field with source term, which can be derived from Maxwell's equations:

$$\nabla^2 \boldsymbol{E} - \frac{1}{(c/n)^2} \frac{\partial^2}{\partial t^2} \boldsymbol{E} = \boldsymbol{F}. \tag{1.2}$$

Here $\boldsymbol{E}$ denotes the electric field, $\boldsymbol{F}$ the source, c the light speed in vacuum, and n the refractive index. When we apply seperations of variables and denote the time-dependent part of $\boldsymbol{E}$ as $e^{-i\omega t}$, where ω denotes the frequency, we can remove the time dependence in (1.2) to obtain

$$\nabla^2 \boldsymbol{E} + n^2 \frac{w^2}{c^2} \boldsymbol{E} = \boldsymbol{F}.$$

Each component of the electric field must then satisfy the following scalar equation, which is known as the inhomogeneous Helmholtz equation:

$$\nabla^2 \phi(\boldsymbol{x}) + k(\boldsymbol{x})^2 \phi(\boldsymbol{x}) = -S(\boldsymbol{x}), \tag{1.3}$$

where we introduced the wavenumber $k(\boldsymbol{x}) = n(\boldsymbol{x})k_0 = n(\boldsymbol{x})\frac{\omega}{c}$, with k_0 the wavenumber in vacuum and $n(\boldsymbol{x})$ the refractive index distribution. We will assume that the refractive

index is real, to have conservation of energy in the wave field. A complex refractive index with positive real part would correspond to absorption by the medium. We also assume that the refractive index is piecewise constant. The source term is denoted as $S(\boldsymbol{x})$.

When we choose $A = \nabla^2 + k^2$, this equation is equivalent to (1.1), with the source equal to $S(\boldsymbol{x}) = -\psi$.

First, in Section 2, a theory about eigenmodes is given, combined with an explanation of quasi-normal modes, which are useful for open cavities. Then, approaches for solving linear systems, including the preconditioning method of [20], are discussed in Section 3. In Section 4 we introduce our method to find eigenmodes and specify how we use the preconditioner and solver in this method. We will then validate and illustrate the performance of the method on the mentioned different cases in Section 5. Finally, the results will be discussed and recommendations are given.

2 Quasi-normal modes

In the study of optical cavities, it is essential to know the resonating frequencies of the cavity. When the cavity is excited at a resonating frequency, energy builds up inside the cavity and thus the scattering behaviour of the cavity is much different than at non-resonant frequencies, because a large part of the incoming wave is transmitted into the cavity instead of being reflected. The wave field in a system at a resonance is called an eigenmode.

An optical system has a number of eigenmodes, in many cases infinitely many. The eigenfunctions corresponding to these eigenmodes are solutions of the wave equation and often form an orthonormal basis for all solutions. For wave equations, we denote eigenmodes as solutions to $A(\omega)\phi = 0$, where $A(\omega)$ is the operator with the eigenvalue dependent on ω incorporated.

Consider for example the homogeneous Helmholtz equation, which is (1.3) without a source:

$$\nabla^2\phi(\boldsymbol{x}) + k^2\phi(\boldsymbol{x}) = 0, \tag{2.1}$$

where we assume k is constant in the domain of the eigenmodes, which is typically the cavity. Solutions to this equation are essentially eigenvalue problems of the Laplace operator, with eigenvalues $-k^2$. For a system, there is a possibly infinite set of eigenvalues and corresponding eigenfunctions that solve this eigenvalue problem.

A property of eigenmodes, for Hermitian operators, is that they are orthogonal and can be normalized to be orthonormal (see [10]). In one spatial dimension, for eigenmodes ϕ_j orthonormality can be stated as

$$\langle\phi_j|\phi_l\rangle = \delta_{jl} \tag{2.2}$$

where $\langle\cdot|\cdot\rangle = \int_{-\infty}^{\infty} |\phi(x)|^2 dx$ denotes the standard $L^2(\mathbb{R})$ inner product on the vector space and δ_{jl} denotes the Kronecker delta function. For Hermitian operators, the set of orthogonal eigenfunctions forms a basis for all possible solutions for the given system. This is what we call completeness. The operator in the Helmholtz equation, $\nabla^2 + k^2$, is not Hermitian on the usual Hilbert space, so completeness does not hold. However, if we define an alternative inner product, completeness holds. This inner product is given and explained below in (2.4).

For a system in which the total energy is conserved, the vacuum wavenumber k_0 and thus the frequency $\omega = k_0 c$ corresponding to eigenmodes, are real. For cavities coupled to the field outside the cavity, where the energy is not conserved inside the cavity, however, it is very helpful to find modes for the cavity, instead of for the universe, which extends to infinite space. According to [12], the modes of a cavity are discrete, with wavenumbers seperated by $\Delta k_0 \sim \pi/L$, with L the spatial dimension of the cavity. If we place the cavity in a universe of size Λ, with $\Lambda \to \infty$ and apply boundary conditions, however, we can formulate the wavefunction in modes of the universe. The wavenumbers are then seperated by $\Delta k_0 \sim \pi/\Lambda$, which means the modes are continuous, since $\Lambda \to \infty$, according to [12]. Therefore, the modes of the universe are difficult to locate and distinguish from each other, making them less useful. Because they are so closely spaced, the influence of a specific mode is hard to distinguish from neighboring modes.

Also, when not using the modes of the cavity, the intuitive connection to the corresponding closed cavity is lost. That is, the modes of the open cavity are the same as modes of a closed cavity in the limit where the contrast between inside and outside the cavity goes to infinity. Therefore, the approach is to use the modes of the cavity to describe the field inside an open cavity.

However, when we want to find the modes of the cavity, we have to keep in mind that cavities with coupling are leaky. That is, energy leaks out of the cavity and is not conserved. We can still find modes for the system, but they are characterized by complex eigenfrequencies and complex wavenumbers. These modes are called quasi-normal modes.

Such eigenfrequencies are complex with strictly negative imaginary parts, such that the energy inside the cavity is damped over time.[1] This is because the eigenmodes are solutions to a system without a source, so no energy enters the cavity. The energy in the cavity will, over time, spread out over the entire space. Therefore the energy inside the cavity decreases over time, so the frequency must have a negative imaginary part.

The quasi-normal modes are still solutions of the eigenvalue problem in (2.1), but now allowing complex ω. Also, they need to be outgoing. Considering the situation in one dimension, that means that for negative x, the eigenfunction looks like $e^{-in\frac{\omega_j}{c}x}$ and for positive x like $e^{in\frac{\omega_j}{c}x}$.

From this outgoing condition it follows that the quasi-normal modes must have the asymptotic form

$$\phi_j(x) = e^{\pm in\frac{\omega_j}{c}x} \to \infty, \quad \text{for } x \to \pm\infty, \tag{2.3}$$

which diverges because $\Im(\omega_j) < 0$. We assume that the refractive index n is real and constant for large $|x|$, thus the cavity is placed inside a homogeneous medium.

Because the quasi-normal modes grow exponentially outwards, using quasi-normal modes puts forth some problems with the orthogonality and completeness of the modes. These do not hold when using the standard inner product and norm. Because of the dissipation of energy out of the cavity, the operator with the cavity as its domain is non-Hermitian. Therefore the orthogonality and completeness of the quasi-normal modes are not guaranteed. However, In [12] it is shown that if we take an alternative definition of the inner product, completeness and orthogonality of the quasi-normal modes hold. This alternative inner product is in one dimension defined as

$$\langle \phi_j | \phi_l \rangle = \int_{-\infty}^{\infty} \left(\frac{n(x)}{c} \right)^2 \phi_j^*(x) \phi_l(x) dx, \tag{2.4}$$

[1] Recall we denote the time dependence as $e^{-i\omega t}$.

where $n(x)$ is the refractive index as a function of space. With this inner product, the $\nabla^2 + k^2$ is Hermitian and thus the eigenvectors form a basis for the cavity. It is important to note that the completeness only holds inside the cavity, while the orthogonality involves the outside, because the integral extends to $|x| = \infty$. For the completeness and orthogonality of the quasi-normal modes to hold, the refractive index distribution must satisfy two conditions, namely that it must have a discontinuity on the boundary of the cavity and that the refractive index must approach a constant asymptotic value sufficiently rapidly, as said in [12]. This conditions essentially imply that we consider a cavity inside a homogeneous medium.

Note that the normality of the modes can not hold with the given inner product, since the modes diverge as $|x| \to \infty$. The normality of quasi-normal modes is only recently proven and research on the completeness is still being done. The review by Lalanne et al. [11] provides more details.

The quasi-normal modes are related to the normal modes of the corresponding isolated cavity. When the contrast between the refractive index inside and outside the cavity is increased, the dissipation decreases and the imaginary part of ω_j becomes less negative. In the limit where the contrast of refractive index goes to infinity, the quasi-normal modes are the same as the normal modes inside the cavity.

The (quasi-normal) modes of a system provide a lot of information about the behaviour of the system. When the system is excited with a frequency that is the same as the eigenfrequency, there will be resonating behaviour. Then we have a strong coupling between the incoming wave and the cavity. The field inside a cavity will thus be much larger when it is excited by frequencies that are eigenfrequencies. This also influences the scattering of the incoming wave, as more energy will be transmitted into the cavity.

More specifically, quasi-normal modes are very useful to study the behavior of open cavities. With open cavities there is leakage to outside the cavity. For such systems, the quasi-normal modes are generally more easy to compute than the normal modes for the entire system, which makes them useful to study the behaviour of open cavities. Therefore it is relevant to look into efficient methods to find the quasi-normal modes.

3 Solving linear systems using a preconditioner

Eigenmodes ϕ are a solution to a specific linear system, namely $A\phi = 0$, where A is an operator. In the method explained in Section 4, we will approximate the eigenmodes by using a source ψ and solve the linear system $A\phi = \psi$. Such a linear system can generally be solved iteratively and in many cases a preconditioner is used to do this efficiently. In this section, the function of such a preconditioner will be explained for the Richardson iteration and more specifically, the universal preconditioner of [20] will be given. A few methods other than the Richardson iteration will be mentioned and finally, the need for absorbing boundaries is explained.

3.1 Richardson iteration with a preconditioner

Many problems in optics can be stated as a linear system, in which there is an invertible operator A which acts on the field ϕ which gets excited with a source ψ. We denote such a system as $A\phi = \psi$.

Here the problem is to find the field ϕ that results from the source ψ, that is, find

the inverse of the operator A. Many different approaches exist to solve such problems. A simple approach is to use the Richardson iteration to converge to a solution, where the m-th iteration is as follows:

$$\phi^{(m+1)} = \phi^{(m)} + \alpha(\psi - A\phi^{(m)}). \tag{3.1}$$

Here α is a parameter that can be tuned to optimize convergence. An initial guess $\phi^{(0)}$ should be given. In each iteration, the residual, multiplied with α, is added to $\phi^{(m)}$. at the point $\phi^{(m)} = \phi$, the residual vanishes, so the iteration has a stationary point at solution ϕ. The method is very memory efficient, as only one solution has to be stored at a time. The iteration method converges if $\|1 - \alpha A\| < 1$, since for the error $e^{(m)} = \phi^{(m)} - \phi$ we have

$$\|e^{(m+1)}\| = \|\phi^{(m)} - \phi + \alpha(A\phi - A\phi^{(m)})\| = \|(1 - \alpha A)e^{(m)}\| \leq \|1 - \alpha A\| \cdot \|e^{(m)}\|.$$

For many systems $\|1 - \alpha A\| < 1$ does not hold, or only for small α, when the convergence becomes very slow. Then a typical approach is to use a preconditioner Γ such that $\|1 - \alpha\Gamma^{-1}A\| < 1$ and we then solve the left-preconditioned system

$$\Gamma^{-1}A\phi = \Gamma^{-1}\psi, \tag{3.2}$$

which, provided that Γ^{-1} is non-singular, has the same solution ϕ as (1.1).

A universal preconditioner was introduced in [20]. This preconditioner works for operators on a Hilbert space that are accretive. An accretive operator has non-negative real part. Formally, accretivity is defined as follows:

$$\Re(A) = \inf_{\phi \in D(A)\setminus\{0\}} \frac{\langle \phi, A\phi \rangle}{\langle \phi, \phi \rangle} \geq 0, \tag{3.3}$$

with $D(A)$ the domain of A. Many non-accretive systems can be transformed into an equivalent accretive form, as described in [20].

Now assume we can split A into an approximation L and discrepancy $V = A - L$ such that $\|V\|<1$. Then the following preconditioner ensures that $\|1-\alpha\Gamma^{-1}A\| < 1$, with tuning parameter $0 < \alpha \leq 1$:

$$\Gamma^{-1} = (1 - V)(L + 1)^{-1}. \tag{3.4}$$

The validity of this preconditioner and the fact that it is universal for all linear systems is proven in [20].

We will specifically look at solving the inhomogeneous Helmholtz equation, using this preconditioner. This problem is also studied in [20]. Vettenburg et al. also argued that the time-harmonic Maxwell's equations can be solved similarly.

We rewrite (1.3) to get out the constant part of the wavenumber k_o, such that $k(\boldsymbol{x})^2 - k_o^2$ has compact support:

$$\nabla^2\phi(\boldsymbol{x}) + k_o^2\phi(\boldsymbol{x}) + (k(\boldsymbol{x})^2 - k_o^2)\phi(\boldsymbol{x}) = \psi(\boldsymbol{x}) \tag{3.5}$$

We can discretize the operator on ϕ by evaluating u at points in a grid and set $A = \nabla^2 + k_o^2 + (k(\boldsymbol{x})^2 - k_o^2)$. The system we then want to solve is

$$A(\omega)\phi = \psi. \tag{3.6}$$

The operator A is dependent on the wavenumber $k(\boldsymbol{x}) = n(\boldsymbol{x})k_0$ and thus on the frequency $\omega = ck_0$.

The form of (3.5) already includes a partition of A into $L+V$. We multiply the system with a constant $c = \frac{-0.95i}{\|k(\boldsymbol{x})^2 - k_o^2\|}$ to make the system accretive and set $V = c(k(\boldsymbol{x})^2 - k_o^2)$ such that we have $\|V\| = 0.95$, which is smaller than 1, as needed. Then $L = c(\nabla^2 + k_o^2)$.

The value of 0.95 for $\|V\|$ was chosen in [20] since the convergence rate was found to not be very sensitive to this value, and 0.95 is slightly less then 1, so the convergence rate can largely be determined with α, which is a measure for the step size in the Richardson iteration method.

The system can only be made accretive if the system is gain-free. That is, if the imaginary part of $k(\boldsymbol{x})^2$ is non-negative, which is, if we use a real refractive index, analogous to the imaginary part of k_0^2 being non-negative. This is equivalent to saying that the frequency ω must have non-negative imaginary part, which is opposite to the complex frequency of a quasi-normal mode. Therefore, the preconditioner can not be used to exactly find the quasi-normal modes, but only find an approximation for real frequencies.

To find the inverse of $L+1 = c(\nabla^2 + (k_o)^2) + 1$, which is needed for the preconditioner of (3.4), we use the Green's function $G(\boldsymbol{x} - \boldsymbol{y})$ for operator $L + 1$. The Green's function for the homogeneous Helmholtz equation is defined as follows (see e.g. [5]):

$$G(\boldsymbol{x} - \boldsymbol{y}) = \begin{cases} \dfrac{ie^{ik|\boldsymbol{x}-\boldsymbol{y}|}}{2k}, & \text{if } d = 1, \\ -\dfrac{i}{4}H_0^{(1)}(k(|\boldsymbol{x} - \boldsymbol{y}|), & \text{if } d = 2, \\ \dfrac{e^{ik|\boldsymbol{x}-\boldsymbol{y}|}}{4\pi|\boldsymbol{x} - \boldsymbol{y}|}, & \text{if } d = 3, \end{cases} \tag{3.7}$$

where d is the number of dimensions and $H_0^{(1)}$ is a Hankel function.

The Green's function $G(\boldsymbol{x} - \boldsymbol{y})$ is then the solution to the following equation:

$$(c\nabla^2 + c(k_o)^2 + 1)G(\boldsymbol{x} - \boldsymbol{y}) = -\delta(\boldsymbol{x} - \boldsymbol{y}) \tag{3.8}$$

By Green's function theorem, using the method described in [14], we can then express the solution to $(L+1)\phi = \psi$ in terms of the Green's function. The integral in the following equation is over Ω, which is the support of ψ and was assumed to be compact.

$$\phi(\boldsymbol{x}) = -\int_\Omega G(\boldsymbol{x} - \boldsymbol{y})\psi(\boldsymbol{y})d\boldsymbol{y} \tag{3.9}$$

Because this integral is a convolution, it is efficient to do this operation in the Fourier domain, where the convolution is just a multiplication. If we take the Fourier transform of (3.8), we get

$$\begin{aligned} (-c\|\boldsymbol{p}\|^2 + ck_o^2 + 1)\mathcal{F}[G(\boldsymbol{x} - \boldsymbol{y})] &= -1 \\ \mathcal{F}[G(\boldsymbol{x} - \boldsymbol{y})] &= -\frac{1}{-c\|\boldsymbol{p}\|^2 + ck_o^2 + 1}, \end{aligned}$$

where $\boldsymbol{p}$ denotes the coordinate vector in Fourier space. Thus, taking the Fourier transform of ψ and multiply it with $\mathcal{F}[G(\boldsymbol{x} - \boldsymbol{y})]$ gives us the Fourier transform of the solution ϕ. Using this, we have for the inverse

$$(L + 1)^{-1} = \mathcal{F}^{-1}\frac{1}{-c\|\boldsymbol{p}\|^2 + ck_o^2 + 1}\mathcal{F}. \tag{3.10}$$

Using the Fast Fourier Transform (FFT) on an evenly spaced grid, the Fourier transform and inverse Fourier transform can be computed efficiently. Because of this, the preconditioner is efficient to compute. In the Richardson iteration, the residual $\Gamma^{-1}\psi - \Gamma^{-1}A(\omega)\phi$ can thus be calculated efficiently. Because we know $\|1 - \alpha\Gamma^{-1}A\| < 1$, the preconditioner can efficiently be used to find solutions to (3.6), with the Richardson iteration.

3.2 Other solvers for linear systems

The preconditioner discussed above is designed to use with the Richardson iteration method and convergence of the Richardson iteration with the preconditioner has been proven. The Richardson iteration method is very simple and memory efficient, however it has some shortcomings. It does not converge when we are at a frequency where there is an eigenmode. At such a frequency ω, there exists a mode ϕ_0 such that $A(\omega)\phi_0 = 0$. Therefore, the norm $\|1 - \alpha A(\omega)\| = \sup_{\phi \in D(A)\setminus\{0\}} \frac{\|(1-\alpha A(\omega))\phi\|}{\|\phi\|} \geq 1$, as it is equal to 1 for $\phi = \phi_0$. Therefore the error will not decrease each iteration, even with the use of a preconditioner.

Other methods exist to find the solution to linear systems. Two of these are the generalized minimal residual method (GMRES) and the biconjugate gradient stabilized method (BiCGSTAB) introduced in [16] and [21], respectively. Those methods are also shown to converge when using the preconditioner (3.4) in practice in [20].

A downside of those methods is that convergence cannot be proven in all cases. Therefore the method might stagnate in some situations. Often, however, the methods perform well. In Section 4 it will be described which iterative method can best be used when locating eigenmodes.

3.3 Absorbing boundaries

When solving a system numerically, it has to be discretized. For closed, finite systems, this can be pretty straightforward, as one can easily partition the domain into a grid. However, when considering a system that is coupled to the outside, an accurate solution would have to take into account the behaviour in the entire universe R^d, with d the dimension of the system. Otherwise, the behavior at the edges of the domain will influence the solution. However, in many cases only the behavior of the field inside a finite domain, e.g. the scattering behavior inside and close to a leaky cavity, is relevant.

In these cases, often an absorbing boundary is used. Such a layer is an artificial boundary layer that is added at the edges of a finite domain. Inside this boundary layer, all waves are absorbed. Such a layer must not reflect waves back into the system. When using such an absorbing boundary layer, the behavior inside the finite domain and thus inside the cavity, is as if the system extends to infinity. Therefore this is a very useful method in cases where we have systems with infinite size.

4 Method for finding modes

We have now stated available methods that are used to find numerical solutions to linear systems efficiently. In this chapter it will be explained how the numerical solutions of a linear system can be used to find modes of the system. In Section 4.2 we will explain how the numerical solutions can best be computed when using the method.

4.1 Finding modes

We want to find the modes of an operator $A(\omega)$. Recall from Section 2, that at or close to a frequency ω at which there is a mode, there is resonating behavior.

To locate the frequencies for which there is resonating behavior, we use an altered version of a method described in [4]. We use the fact that an eigenmode ϕ satisfies $A(\omega)\phi = 0$. When at an eigenfrequency ω_0, we thus have that $A(\omega_0)$ is singular. Therefore, $\|A^{-1}(\omega)\psi\| \to \infty$ if $\omega \to \omega_0$ for any non-zero vector ψ, except for the case where ψ is orthogonal to the eigenvector ϕ corresponding to ω_0. We define the following function:

$$f(\omega) = \frac{1}{\|A^{-1}(\omega)\psi\|}, \tag{4.1}$$

where ψ is a fixed random vector. Because it is random, it will, except in a very unlikely scenario, not be orthogonal to the eigenvector ϕ. Since $\|A^{-1}(\omega)\| \to \infty$ when ω approaches an eigenfrequency, this function vanishes at eigenfrequencies.

The vector $A^{-1}(\omega)\psi$ is the solution ϕ to the system $A(\omega)\phi = \psi$. We can solve this system numerically and evaluate $f(\omega)$. To solve this system efficiently, the preconditioner can be used. Because of numerical precision, we do not expect to find values ω for which $f(\omega)$ evaluates exactly to 0. However, close to a resonance, we expect to see a minimum of the function. The problem of finding eigenfrequencies thus reduces to finding minima of a function of one variable. These eigenfrequencies can in principle be complex, and for the case of quasi-normal modes of an open system, have negative imaginary part.

When using the preconditioner, we only evaluate $f(\omega)$ for real ω. This is because the preconditioner is only effective when the system is accretive, which is not the case for ω with negative imaginary part. The behavior of $f(\omega)$ on the real axis does correspond well with the behavior in the complex plane, since the oscillating behavior is the same. The imaginary part only adds an exponential growth to the amplitudes of the oscillations. This will be further illustrated with the case of a Fabry-Perot resonator in Section 5.1. Therefore the real resonating frequencies can still be found when looking for minima of $f(\omega)$. The real frequency is not an exact eigenfrequency, but is useful in practice, as we can only excite the system with a wave with real frequency.

The random vector ψ represents a random source for the system. Because it is random, the eigenmodes will very likely be excited by the source, if they are present. Only if the source is orthogonal to the eigenmode, the eigenmode will not be excited. The eigenmodes will resonate, making the norm $\|A^{-1}(\omega)\psi\|$ large. It will not completely go to infinity however, since the used frequency is not the exact eigenfrequency. Thus, also other modes contribute to the solution ϕ, which do not satisfy $A(\omega)\phi = 0$.

The randomness of ψ can be chosen in different manners. A simple approach is to simply use white noise by setting a random value at each entry of ψ. Also for some systems, plane waves coming from different directions can be used and achieve better results than white noise. In Section 5, both kinds of random vectors are used.

When a frequency has been found for which $f(\omega)$ has a minimum, the used solver can also be used to find the solution ϕ to the system, again using a random source. Because the eigenmode will resonate, it forms the main part of the solution. Thus, the found solution ϕ is a good approximation of the eigenfunction. Because not the exact eigenfrequency is used, the solution will never be the exact eigenfunction. Other eigenfunctions also contribute to the solution.

To find a minimum of $f(\omega)$, we used Matlab's `fminsearch` function (see [6]). This function finds local minima of an arbitrary function. Here the initial guess was chosen based on a line search, from which the minima can be guessed by looking at the graph. Then the minimizer function is used to refine this guess and find an accurate result. Other minimizer methods can also be used.

4.2 Numerical simulations

The numerical solutions used to evaluate $f(\omega)$ can be found using the universal preconditioner stated in Section 3. The system $A\phi = \psi$ can be initialized in the environment AnySim of [20], where also the preconditioned operator $\Gamma^{-1}A$ is constructed.

In AnySim, there is the option to include absorbing boundaries, which we used when finding numerical solutions. There the Nuttal window function, introduced in [13], is used to decrease the function to 0. The width of the absorbing boundaries should be large enough, that is, in the order of 10 wavelengths, to not influence the behavior inside or close to the cavity.

As said in Section 3, the Richardson iteration does not converge at a resonance. Therefore we resorted to GMRES and BiCGSTAB. When looking to find numerical approximations of quasi-normal modes, it was found that GMRES, like the Richardson iteration, did converge very slowly close to a resonating frequency and did not converge at all when exactly at a resonance. For BiCGSTAB, the convergence was slightly slower when the frequency was close to a resonating frequency than in cases where there was no resonating behavior, but the convergence was still fast. Therefore we chose to use BiCGSTAB to find numerical solutions to the preconditioned system. This method is not proven to converge in all situations and might in theory stagnate. However, we found that is was robust and accurate in all cases we studied.

We thus use AnySim to construct the preconditioned operator, which we solve using BiCGSTAB. Here the source is a random source, consisting of white noise or random plane waves, depending on the case.

These numerical solutions are used to compute $f(\omega)$ and find its minima. After that, it can be used to find the solutions ϕ at the resonating frequencies. This solutions ϕ are an approximation of the eigenmodes.

5 Numerical experiments

To verify the effectiveness and accuracy of the method at finding modes, we test it on two different setups. We approximate the eigenmodes of the homogeneous Helmholtz equation (2.1). First we look at a Fabry-Perot resonator in one dimension in Section 5.1 and then we look at a dielectric circular cavity in two dimensions in Section 5.2. Both are relatively simple systems, in the sense that we can find the modes or solutions of the system analytically and compare with the results of our method using AnySim.

To show that the method also works for other cavities, for which an analytical solution does not exist, it is applied on a deformed circular cavity. This way, a practical use of the method is illustrated.

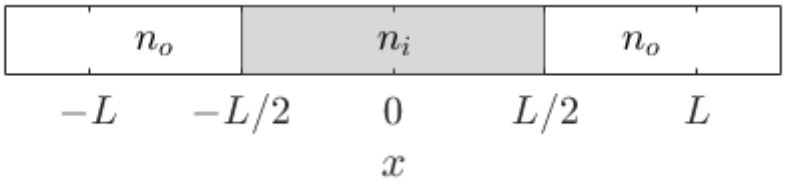

FIGURE 5.1: Setup for a Fabry-perot resonator in one dimension, with refractive index n_i inside and n_o outside the cavity.

5.1 1D case: Fabry-Perot resonator

5.1.1 Setup

We analyze a Fabry-Perot resonator in one dimension of length $L > 0$, which consists of a cavity inside a homogeneous medium. This can be represented by the following expression for the refractive index, where we assume the refractive index is piecewise constant and independent of frequency.

$$n(x) = \begin{cases} n_i, & \text{for } |x| < L/2 \\ n_o, & \text{for } |x| \geq L/2 \end{cases} \tag{5.1}$$

The refractive index can in general be complex, but we use real refractive index for simplicity. The ambient medium is often taken as vacuum, such that $n_0 = 1$. We denote the wavenumber inside as $k_i = n_i k_0$ and outside as $k_o = n_o k_0$. The setup is illustrated in Figure 5.1.

5.1.2 Derivation of quasi-normal modes

The derivation of the quasi-normal modes is based on [11]. To find the modes, we first write a general expression for the field. When there is no incident wave, the field can be written as a superposition of two waves propagating in opposite direction inside the cavity. Outside the cavity we have two outgoing plane waves. At complex frequency $\omega = ck_0$, with c denoting the light speed and k_0 denoting the complex wavenumber in vacuum, we then have the the total field given by

$$\phi(x) = \begin{cases} Ae^{ik_i x} \pm Ae^{-ik_i x}, & \text{for } |x| < L/2 \\ Be^{ik_o x}, & \text{for } x \geq L/2 \\ \pm Be^{-ik_o x}, & \text{for } x \leq -L/2 \end{cases} \tag{5.2}$$

Here A and B are the complex field amplitude inside and outside the cavity, respectively. The plus symbols correspond to modes that are symmetric with respect to the center of the cavity, while the minuses correspond to anti-symmetric modes.

If there is a resonance, the field amplitude should be the same after a round trip in the cavity. The round trip is two times the length of the cavity L and includes 2 reflections at the boundary. Analytically, this gives the following condition:

$$A = Ar^2 e^{2ik_i L}. \tag{5.3}$$

Here, the reflection coefficient r is given by the Fresnel equation for normal incidence (see, e.g., [15]):

$$r = \frac{n_i - n_o}{n_i + n_o}.$$

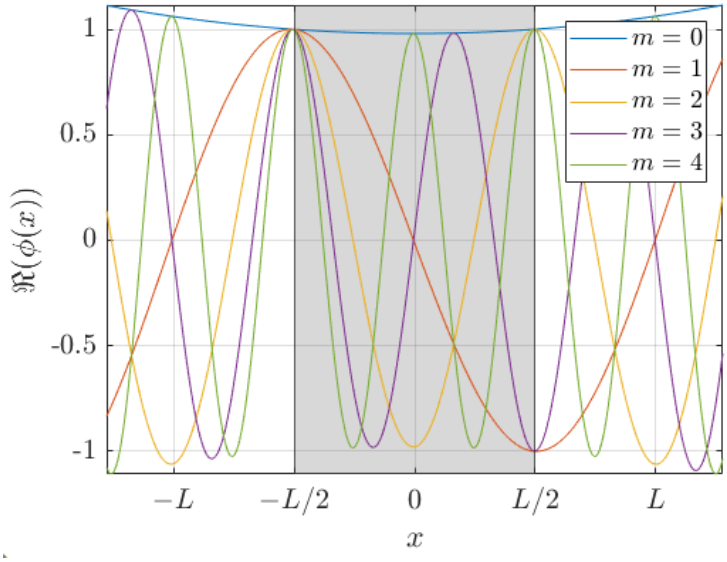

FIGURE 5.2: The real part of the quasi-normal modes in a Fabry-Perot resonator with $m = 0$ until $m = 4$. Modes are given by (5.2) with frequencies given by (5.4). $n_i = 5, n_0 = 1$ (other real refractive index only changes the rate of exponential growth). The modes are normalized to have amplitude 1 at the boundaries of the cavity.

In the cavity we lose energy via leakage, as $|r| < 1$. Therefore, condition (5.3) can only be satisfied for complex frequency $\omega = ck_0$, since n is real. The imaginary part of the frequency then restores the stationary state by amplifying the waves and compensating the loss via leakage.

Equation (5.3) can only hold if $e^{2ik_iL} = \frac{1}{r^2}$. Therefore, using the complex logarithm, we then find that the resonant frequency ω_m satisfies:

$$\omega_m \frac{n_i L}{c} = m\pi + i\mathrm{Ln}\,(r)\,, \quad m \in \mathbb{Z}. \tag{5.4}$$

It was shown by Lalanne et al. in [11] that this set of frequencies is complete inside the cavity, which follows from the fact that the Helmholtz equation is Sturm-Liouville. Recall that completeness means that the modes are orthogonal under the inner product of (2.4) and form a basis for all functions inside the cavity. The first few modes are plotted in Figure 5.2. As can be seen in that figure, the modes with even order m are symmetric with respect to the center of the cavity, while for odd m the modes are anti-symmetric.

The amplitude of the modes grows exponentially when going outwards from the origin. The mode with $m = 0$ has no oscillating behavior and is the envelope in which all oscillating modes are contained.

In (5.4) we see that $\Im(k_i) = \Im(\omega_m \frac{n_i}{c}) < 0$. Thus, $|\phi(x)|$ as given by (5.2) grows exponentially for increasing $x > L/2$ and decreasing $x < -L/2$. All modes grow with the same rate, since the imaginary part of ω_m is not dependent on m. Because of this exponential growth, the modes cannot form a basis for the field outside the cavity. This is expected, since the quasi-normal modes are defined to be modes of a cavity that is connected to outside. They are not modes of the entire system including the outside, but only represent the field inside the cavity. The negative imaginary part of ω_m shows that the energy inside the cavity decreases over time, as was discussed in Section 2.

5.1.3 Numerical results

We now apply AnySim to approximate the modes numerically, using the method described in Section 4. We compute solutions to the inhomogeneous Helmholtz equation (1.3) numerically using the preconditioner of AnySim and the BiCGSTAB solver. Because the preconditioner only produces a well-conditioned problem for accretive operators, as described in Section 3, and the Helmholtz equation is only accretive for frequencies with non-negative imaginary part, we will not be able to find the exact complex quasi-normal mode frequencies that we are looking for, which have negative imaginary part. Therefore we look for approximate frequencies on the real axis, and assume that the behavior on the real axis is an accurate projection of the behavior in the complex plane. The solutions with complex frequencies have the same oscillating behavior as the real frequencies with equal real part, but have an exponantial growth or decay, which solutions with real frequencies do not have. Since the oscillations are similar for equal real part, the resonating behavior, which happens at frequencies where the roundtrip length in the cavity is a multiple of the real part of the wavelength, will take place for equal real part. We will see from our results that this is indeed the case.

To find a numerical solution using AnySim, combined with BiCGSTAB, we use its environment HelmholtzSim, to produce a preconditioned operator. Then BiCGSTAB is used to compute a solution for the system with this operator and a random source. For this case, we choose the random source as white noise. That is, the source has a random value at each grid point. This way, we expect to be able to excite the resonant modes, as was explained in Section 4.

We use the following parameters: We set $n_i = 5$ and $n_o = 1$, to have a high contrast between inside and outside the cavity and thus stronger resonances. The resolution is $2\mu m^{-1}$ and the total system has size $256\mu m$, with the length of the cavity being $L = 100\mu m$. For the absorbing boundaries the Nutall window function is used, with a boundary width of $1024\mu m$ on both sides. The achieved solutions for a few frequencies are plotted in Figure 5.3.

Clearly, in Figure 5.3 we see that the amplitude of the solution is much larger outside the cavity than inside. This is caused by the random source. Outside, the refractive index is smaller and thus the wavelength is larger than inside. Because of that, more grid points with white noise fit into a single wavelength. The solution ϕ as a convolution with the Green's function in (3.9) performs as a band-pass filter around wavenumber k. Because for smaller k, more white noise fits into a wavelength, more noise is not filtered in the solution and the amplitude of the solution is larger. Thus, the effects visible in the figure are caused by the random source.

Inside, the wave function has a constant amplitude and shows almost constant oscillating behavior. We look at the behavior inside the cavity, and that does not seem to be influenced by the large wave intensity outside the cavity. For $\omega = 3.00 \times 10^{13}\text{rad}/s$, the amplitude is the largest, so this frequency will be close to a resonance.

To find the modes, we minimize the function

$$f(\omega) = \frac{1}{\|\phi\|_{|x|<L/2}}, \tag{5.5}$$

where $\|\cdot\|_{|x|<L/2}$ denotes the L^2-norm over the cavity $|x| < L/2$, which on a one-dimensional grid is the square root of the solution vector inside the cavity transposed and conjugated times itself. The function $f(\omega)$ that we get is plotted in Figure 5.4.

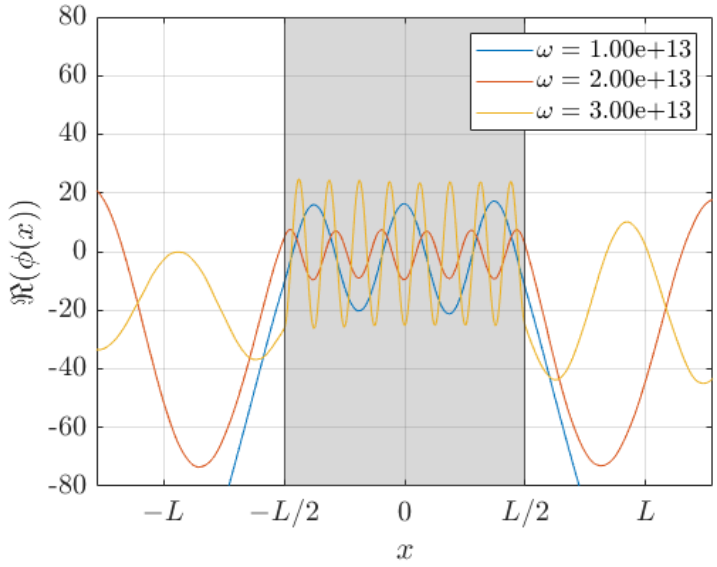

FIGURE 5.3: The real part of the numerical solution using AnySim for the Helmholtz equation on a Fabry-Perot resonator for different frequencies. $n_i = 5, n_o = 1$ and $L = 100\mu m$. The resolution is $1\mu m^{-1}$. The source is white noise.

The first thing we notice in Figure 5.4 is that there is a significant noise component in $f(\omega)$ for higher frequencies. That is, the numerical value of $f(\omega)$ oscillates sharply around its more continuous average shape. This noise is not caused by using random source as an input, since the random noise is constant for all frequencies. However, the noise has to do with the resolution of the grid. For higher frequencies, the number of pixels per wavelength decreases, since the total number of pixels remains constant. Therefore, the size of one pixel corresponds to a larger portion of a wave. One pixel thus makes a larger difference between resonating and non-resonating behavior. This causes that $f(\omega)$ is computed with lower accuracy.

Since the function $f(\omega)$ uses a random source ψ, the results may differ between different experiments. However, the function $f(\omega)$, especially around its minima, remained very similar for different random ψ. Thus, the results are not significantly dependent on ψ.

Additionally, in Figure 5.4 we see that minima of $f(\omega)$ often correspond to the real part of the frequencies of the quasi-normal modes, which are at the vertical lines. Especially the minima corresponding to even values of m, that are symmetric modes, are well visible. Because most minima are very close to the real part of the quasi-normal mode frequency, we can conclude that the behavior of the system for real wavelength is an accurate projection of the behavior in the entire complex plane.

The anti-symmetric modes are less well visible, especially for lower frequencies. At those frequencies, a local minimum is not or barely visible. Apparently, the way the modes are excited with the random source, does not work well for large wavelength anti-symmetric modes.

Let us now find the numerical solutions corresponding to the first few modes. These are displayed in Figure 5.5. When comparing with the modes in Figure 5.2, we see that the even modes ($m = 2, 4$) of the numerical solution are very similar to the analytic modes. The odd modes ($m = 1, 3$), however, are not similar. They are both shifted about a quarter wavelength and have a peak instead of a zero at $x = 0$. They are not anti-symmetric, as

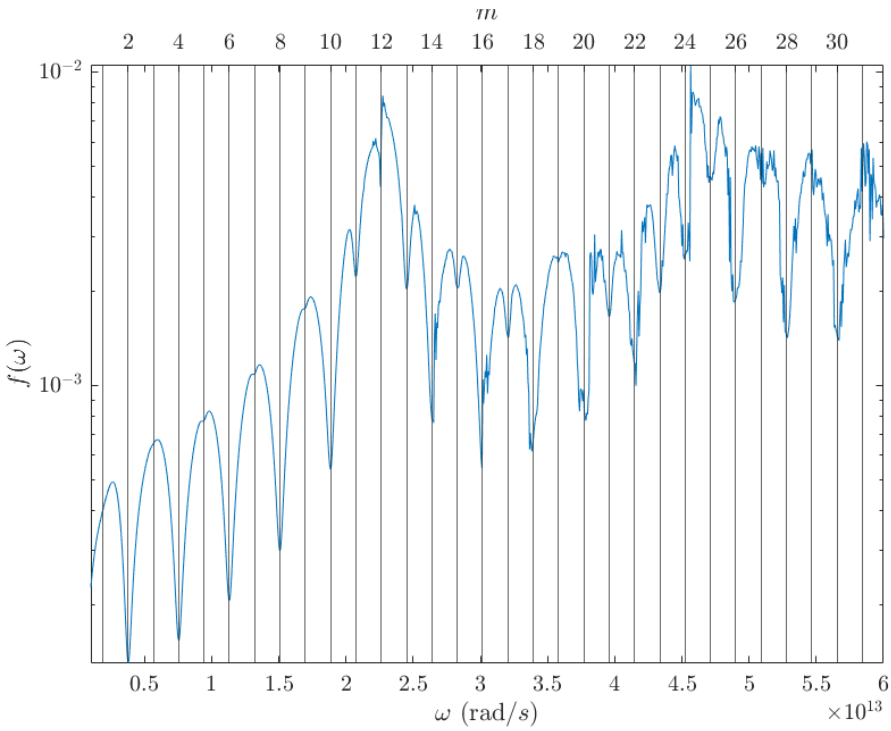

FIGURE 5.4: $f(\omega)$ for a Fabry-Perot resonator, found from the numerical solution using AnySim. $n_i = 5, n_o = 1$ and $L = 100\mu m$. The resolution is $1\mu m^{-1}$. The source is random noise that is the same for each ω. The vertical lines are the real part of the frequencies of the quasi-normal modes, which are given in (5.4).

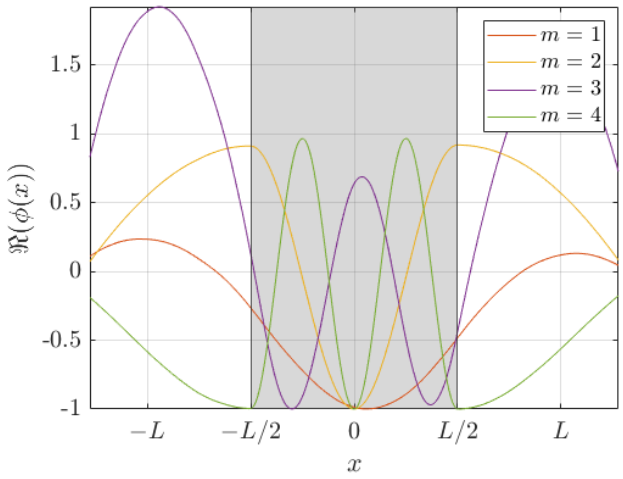

FIGURE 5.5: Numerical solution using AnySim-BiCGSTAB for the Fabry-Perot resonator at the real part of quasi-normal mode frequencies for the first 4 modes, excluding $m = 0$. The wave functions are normalized. $n_i = 5, n_o = 1$ and $L = 100\mu m$. The resolution is $1\mu m^{-1}$. The source is random noise that is the same for each ω.

would be expected for odd modes. In Figure 5.4, we already noticed that there were no minima at frequencies with a low, odd value for m. The low frequency anti-symmetric

modes are not excited by the chosen wave source and are not found in the numerical solution. Therefore they do not lead to a minimum of $f(\omega)$.

Using the MatLab `fminsearch` function, we can find the minima of $f(\omega)$. We look only at real ω values and we set an initial guess based on the plot in Figure 5.4. This initial guess can then be refined by minimizing to find a real frequency that we expect should correspond to the real part of the quasi-normal mode frequency.

The analytical quasi-normal mode frequencies can be compared with the numerically achieved results presented in Table 1. Here we see again that the minimum is not found for a number of odd modes, mostly with low m values. For higher and even m values, on the other hand, the relative error is quite small. Of the 23 cases a minimum was found, 20 are within 2% of the analytical values of ω_m and all are within 3%.

For the found frequencies, the method can approximate the eigenfunction. This approximation will never by exact, since we include a source and we use real frequencies, so the exact quasi-normal modes can not be found. In Figure 5.5, we see that for $m = 2$ and $m = 4$, the amplitude is not exponentially increasing, for example. The found solution also includes parts of other modes and therefore is different from the specific quasi-normal mode. However, the approximations are still accurate, especially the oscillatory behavior where the exponentially growing amplitude is ignored.

We can conclude that for the case of a Fabry-Perot resonator, our method is quite an accurate method to find resonant frequencies, for modes that are symmetrical or of high order. It gives an approximation of the quasi-normal modes, which is not exact since we do not include complex frequencies. The oscillations are similar, however. For anti-symmetric modes, the method works less well and often does not find the mode, because the mode is not excited by the white noise source in the numerical solution.

5.2 2D case: dielectric circular cavity

To validate that our method also works for other problems that involve the Helmholtz equation, we look at a simple setup in two dimensions. It is useful to have a setup for which the solutions can be calculated analytically. Therefore we will look at a dielectric circular cavity in the 2D plane. The goal is to find the resonating frequencies of the cavity. We will look in the real domain for these frequencies.

First, the setup will be explained and the analytical solution for the system will be derived. Then the approach using the method given in Section 4 is given and the results are compared with results found from the analytical solution.

5.2.1 Setup

The setup in two dimensions consists of plane waves scattering on a dielectric circular cavity of radius $R > 0$. This cavity is an area in which the refractive index is different than outside the cavity. We assume it is piecewise constant and independent of wavelength. In polar coordinates, we denote this as follows:

$$n(r,\theta) = \begin{cases} n_i, & \text{if } r < R \\ n_o, & \text{if } r \geq R. \end{cases} \tag{5.6}$$

Here both n_i and n_o can be complex, but we use real refractive index again. $n_o = 1$ represents vacuum. Again, we denote the wavenumber inside and outside the cavity as $k_i = n_i k_0$ and $k_o = n_o k_0$, respectively. The setup is illustrated in Figure 5.6.

m	$\Re(\omega_m))$ (rad/s)	$\text{argmin}_\omega f_{\text{Num.}}(\omega)$ ($\pm 0.001 \times 10^{13}$ rad/s)	Rel. err.
1.000	0.188×10^{13}	not found	NaN
2.000	0.377×10^{13}	0.374×10^{13}	0.008
3.000	0.565×10^{13}	not found	NaN
4.000	0.754×10^{13}	0.741×10^{13}	0.017
5.000	0.942×10^{13}	not found	NaN
6.000	1.131×10^{13}	1.104×10^{13}	0.024
7.000	1.319×10^{13}	1.304×10^{13}	0.012
8.000	1.508×10^{13}	1.524×10^{13}	0.011
9.000	1.696×10^{13}	not found	NaN
10.000	1.885×10^{13}	1.914×10^{13}	0.016
11.000	2.073×10^{13}	not found	NaN
12.000	2.262×10^{13}	2.282×10^{13}	0.009
13.000	2.450×10^{13}	not found	NaN
14.000	2.639×10^{13}	2.611×10^{13}	0.010
15.000	2.827×10^{13}	2.891×10^{13}	0.022
16.000	3.016×10^{13}	3.003×10^{13}	0.004
17.000	3.204×10^{13}	3.297×10^{13}	0.029
18.000	3.393×10^{13}	3.367×10^{13}	0.008
19.000	3.581×10^{13}	3.585×10^{13}	0.001
20.000	3.770×10^{13}	3.823×10^{13}	0.014
21.000	3.958×10^{13}	3.962×10^{13}	0.001
22.000	4.147×10^{13}	4.171×10^{13}	0.006
23.000	4.335×10^{13}	4.259×10^{13}	0.018
24.000	4.524×10^{13}	4.552×10^{13}	0.006
25.000	4.712×10^{13}	4.640×10^{13}	0.015
26.000	4.901×10^{13}	4.806×10^{13}	0.019
27.000	5.089×10^{13}	5.091×10^{13}	0.000
28.000	5.278×10^{13}	5.216×10^{13}	0.012
29.000	5.466×10^{13}	5.487×10^{13}	0.004
30.000	5.655×10^{13}	5.593×10^{13}	0.011

TABLE 1: Minima of $f(\omega)$ found by the numerical solution to the Helmholtz equation for a Fabry-Perot resonator, compared with the analytical quasi-normal mode frequency of the first 30 modes. The minima in column 3 were found using Matlab function `fminsearch` (see [6]) setting the value in column 2 as initial guess. In the cases a minimum was found, this initial guess could also have been chosen based on Figure 5.5. $n_i = 5, n_o = 1$ and $L = 100\mu m$. The resolution is $1\mu m^{-1}$. The source is random noise that is the same for each ω.

We solve the Helmholtz equation both numerically, using the method described in Section 4, and analytically. As the source, we let plane waves with a single frequency enter the system to excite the resonant modes. We use plane waves because then the analytical solution exists [22]. These plane waves go into a random direction and have random phase and amplitude. By superposing many different such random plane waves, it is expected that the resonant modes of the systems will be excited.

5.2.2 Analytical solution

We will now derive the analytical solution for the Helmholtz equation for this setup. We start with the homogeneous Helmholtz equation in 2D. At this stage, we do not use a source term, as we can introduce the source in the solution later. For the circular setup, we use polar coordinates, for which the Helmholtz equation is as follows:

$$\nabla^2\phi(x,y) + k^2\phi(x,y) = \frac{1}{r}\frac{\partial}{\partial r}\left(r\frac{\partial\phi(r,\theta)}{\partial r}\right) + \frac{1}{r^2}\frac{\partial^2\phi(r,\theta)}{\partial\theta^2} + k^2\phi(r,\theta) = 0, \tag{5.7}$$

where ∇^2 is the Laplace operator, ϕ the wave function and $k = k(r) = n(r)k_0$ the wavenumber, which is piecewise constant.

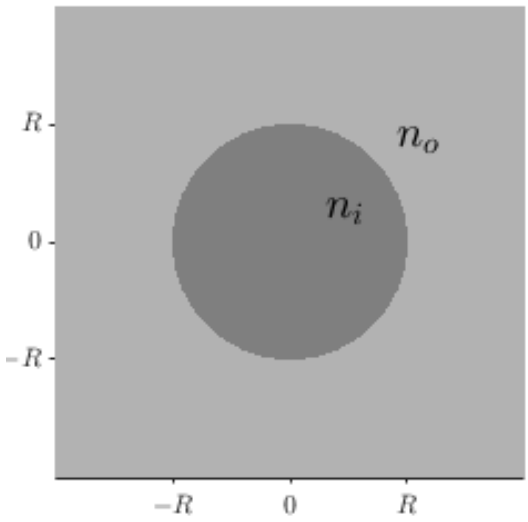

FIGURE 5.6: The setup for a dielectric circular cavity in two dimensions, with refractive index equal to n_i inside and n_o outside.

We use separation of variables to define

$$\phi(r,\theta) = R(r)\Theta(\theta).$$

We substitute this into the Helmholtz equation to obtain

$$\frac{r^2}{R(r)}\left(\frac{1}{r}\frac{d}{dr}\left(r\frac{dR(r)}{dr}\right) + k^2 R(r)\right) = -\frac{1}{\Theta(\theta)}\frac{d^2\Theta(\theta)}{d\theta^2} = \nu^2, \tag{5.8}$$

since the left part is only dependent on r and the right part only on θ, so both sides must be equal to a constant ν^2.

For $\Theta(\theta)$ we then solve the following differential equation:

$$\frac{d^2\Theta(\theta)}{d\theta^2} = -\nu^2\Theta(\theta),$$

which has the general solution

$$\Theta(\theta) = Ae^{i\nu\theta}, \quad \nu \in \mathbb{Z}. \tag{5.9}$$

The order ν is an integer because $\Theta(0) = \Theta(2\pi)$. Here we also see why the constant $\nu^2 > 0$. Otherwise, Θ would be an exponential with real exponent and would not be able to satisfy $\Theta(0) = \Theta(2\pi)$.

For the part dependent on r, we obtain

$$r\frac{d}{dr}\left(r\frac{dR(r)}{dr}\right) + (k^2r^2 - \nu^2)R(r) = 0, \quad \nu \in \mathbb{Z}.$$

We now apply the product rule and substitute $\tilde{r} = kr$. We also define $\tilde{R}(\tilde{r}) = R(\tilde{r}/k) = R(r)$.

$$\tilde{r}^2\frac{d^2\tilde{R}(\tilde{r})}{d\tilde{r}^2} + \tilde{r}\frac{d\tilde{R}}{d\tilde{r}} + (\tilde{r}^2 - \nu^2)\tilde{R} = 0, \quad \nu \in \mathbb{Z}. \tag{5.10}$$

This is a well-known differential equation, namely Bessel's equation (see [2]). There are two kinds of solutions to this equation, namely Bessel functions of the first and second kind, respectively. Linear combinations of those form the general solution to Bessel's equation. We denote Bessel functions of the first kind as $J_\nu(x)$ and of the second kind as $Y_\nu(x)$, where $\nu \in \mathbb{C}$ is the order.

Because these are solutions to the differential equation (5.10), linear combinations of these Bessel functions are also solutions. We choose to use the Bessel functions of the first kind and the Hankel functions of the first kind as fundamental solutions, where the Hankel function is given below. We use the Hankel function of the first kind instead of the Bessel function of the second kind because the Hankel function satisfies the Sommerfeld radiation condition, which we will show later.

$$H_\nu^{(1)}(x) = J_\nu(x) + iY_\nu(x), \quad \nu \in \mathbb{C}. \tag{5.11}$$

We already found that ν must be integer, so the general solution to (5.10) with complex coefficients B and C is then given by

$$R(r) = BJ_\nu(kr) + CH_\nu^{(1)}(kr), \quad \nu \in \mathbb{Z}. \tag{5.12}$$

Combining equations (5.9) and (5.12) we get the general solution to the Helmholtz equation (5.7):

$$\phi(r,\theta) = \sum_{\nu=-\infty}^{\infty} \left[D_\nu J_\nu(kr) + E_\nu H_\nu^{(1)}(kr) \right] e^{i\nu\theta}. \tag{5.13}$$

We can now find the coefficients D_ν and E_ν for both inside and outside the cavity. To do this we make use of the boundary conditions on the edge of the cavity and at infinity. We also include the incoming source wave.

We start by looking inside the cavity, $r < R$. Here the refractive index is equal to n_i. The Hankel functions, $H_\nu^{(1)}(kr)$, have a singularity at the origin ($r = 0$), because the Bessel functions of the second kind have a singularity at the origin. Since the wave function must be finite, these functions cannot be part of the solution inside the cavity.

We thus have

$$\phi_i(r,\theta) = \sum_{\nu=-\infty}^{\infty} D_\nu^i J_\nu(k_i r) e^{i\nu\theta}, \quad \text{if } r < R, \tag{5.14}$$

where the coefficients D_ν^i are determined by the boundary conditions on the edge of the cavity.

Outside the cavity, $r > R$, the refractive index is defined as n_o. We denote the coefficients of the Bessel and Hankel functions outside the cavity by D_ν^o and E_ν^o, respectively. Both the Bessel and Hankel functions are finite outside the origin and thus can be part of the solution outside the cavity. However, we have to take the Sommerfeld radiation condition into account. In two dimensions, this condition is given by

$$\lim_{r\to\infty} r^{1/2} \left(\frac{\partial}{\partial r} - ik(r) \right) \phi_s(r,\theta) = 0 \tag{5.15}$$

where ϕ_s is the scattered wave function. Note that $k(r) = k_o$ for large r.

We will now look at the behaviour of the Bessel and Hankel functions and their derivatives for large r. According to [2], the following asymptotic expansions hold for the Bessel

functions and Hankel function for large $k_o r$:

$$\begin{aligned} J_\nu(k_o r) &\approx \sqrt{\frac{2}{\pi k_o r}} \cos\left[k_o r - \left(v + \frac{1}{2}\right)\frac{\pi}{2}\right], && 8k_o r \gg 4\nu^2 - 1 \\ H_\nu^{(1)}(k_o r) &\approx \sqrt{\frac{2}{\pi k_o r}} \exp\left\{i\left[k_o r - \left(v + \frac{1}{2}\right)\frac{\pi}{2}\right]\right\}, && 8k_o r \gg 4\nu^2 - 1. \end{aligned} \tag{5.16}$$

Note that $J_\nu(k_o r)$ is equal to the real part of $H_\nu^{(1)}(k_o r)$. From these equations we get the following expressions for the asymptotic expansion of the derivative with respect to r:

$$\begin{aligned} \frac{\partial}{\partial r} J_\nu(k_o r) &\approx -k_o \sqrt{\frac{2}{\pi k_o r}} \sin\left[k_o r - \left(v + \frac{1}{2}\right)\frac{\pi}{2}\right], && 8k_o r \gg 4\nu^2 - 1 \\ \frac{\partial}{\partial r} H_\nu^{(1)}(k_o r) &\approx k_o i \sqrt{\frac{2}{\pi k_o r}} \exp\left\{i\left[k_o r - \left(v + \frac{1}{2}\right)\frac{\pi}{2}\right]\right\} && \approx i k_o H_\nu^{(1)}(k_o r), \\ & && 8k_o r \gg 4\nu^2 - 1. \end{aligned} \tag{5.17}$$

When we then refer back to (5.15), we see that $J_\nu(k_o r)$ does not satisfy the Sommerfeld radiaton condition, while $H_\nu^{(1)}(k_o r)$ does. This means that the Bessel functions of the first kind cannot be used to represent outgoing waves. Therefore, we use them to represent the incoming waves. We assume the incoming waves are plane waves with wavenumber k, such that we can use the Jacobi-Anger expansion, which is given by the following identity (see e.g. [5], page 75):

$$e^{ik_o r \cos\theta} = \sum_{\nu=-\infty}^{\infty} i^\nu J_\nu(k_o r) e^{i\nu\theta}. \tag{5.18}$$

This represents a plane wave in the $\theta = 0$ direction. To describe plane waves going into a direction $\theta_0 \in [0, 2\pi]$, with amplitude $\mathcal{A} \in \mathbb{R}$ and with phase shift $\varphi \in [0, 2\pi]$, we have the following:

$$\mathcal{A} e^{i(k_o r \cos(\theta - \theta_0) + \varphi)} = \mathcal{A} e^{i\varphi} \sum_{\nu=-\infty}^{\infty} i^\nu e^{-i\nu\theta_0} J_\nu(k_o r) e^{i\nu\theta}. \tag{5.19}$$

In order to excite the resonant modes inside the cavity, we use N incoming plane waves from different directions $\theta_j \in [0, 2\pi]$, with different amplitudes $\mathcal{A}_j \in \mathbb{R}$ and with different phase shifts $\varphi_j \in [0, 2\pi]$, $j = 1, 2, \ldots, N$. That means that in (5.13), for outside the cavity, the coefficients of the Bessel functions of the first kind are given by

$$D_\nu^o = \sum_{j=1}^{N} \mathcal{A}_j e^{i\varphi_j} i^\nu e^{-i\nu\theta_j}. \tag{5.20}$$

To find the expressions for D_ν^i and E_ν^o we use the following boundary conditions on the solution inside the cavity ϕ_i and outside the cavity ϕ_o to have continuity and differentiability at the boundary $r = R$:

$$\begin{aligned} &\phi_i(k_i R, \theta) = \phi_o(k_o R, \theta) && \text{continuity condition,} \\ &\frac{\partial}{\partial r}\phi_i(k_i R, \theta) = \frac{\partial}{\partial r}\phi_o(k_o R, \theta) && \text{differentiability condition.} \end{aligned} \tag{5.21}$$

These conditions arise from the fact that the electromagnetic field tangential to the boundary between two dielectrics is continuous: it is the same inside and outside the cavity (see e.g. [7]).

Because the boundary conditions must hold for all $\theta \in [0, 2\pi]$, we apply them separately for each ν. We then get

$$\begin{aligned} D^i_\nu J_\nu(k_i R) &= D^o_\nu J_\nu(k_o R) + E^o_\nu H^{(1)}_\nu(k_o R) && \text{continuity condition,} \\ k_i D^i_\nu J'_\nu(k_i R) &= k_o D^o_\nu J'_\nu(k_o R) + k_o E^o_\nu H^{(1)\prime}_\nu(k_o R) && \text{differentiability condition.} \end{aligned}$$

This system can be solved for D^i_ν and E^o_ν:

$$\begin{aligned} E^o_\nu &= D^o_\nu \frac{\frac{J_\nu(k_o R)}{J_\nu(k_i R)} - \frac{k_o J'_\nu(k_o R)}{k_i J'_\nu(k_i R)}}{\frac{k_o H^{(1)\prime}_\nu(k_o R)}{n J'_\nu(k_i R)} - \frac{H^{(1)}_\nu(k_o R)}{J_\nu(k_i R)}} = D^o_\nu C^o_\nu, \\ D^i_\nu &= D^o_\nu \frac{J_\nu(k_o R) + C^o_\nu H^{(1)}_\nu(k_o R)}{J_\nu(k_i R)} = D^o_\nu C^i_\nu, \quad \nu \in \mathbb{Z}. \end{aligned} \tag{5.22}$$

We define C^o_ν as the coupling coefficient between the incoming wave and the scattered wave and C^i_ν as the coupling coefficient between the incoming wave and the wave inside the cavity.

We thus have found an analytical solution for the Helmholtz equation for plane waves incoming on a dielectric circular cavity. We summarize the findings in a theorem.

Theorem 1 *Let* $n(r) = \begin{cases} n_i, & \text{if } r < R \\ n_o, & \text{if } r \geq R \end{cases}$ *be the refractive index for a dielectric circular cavity of radius* R *in two dimensions, and let* $k_i = n_i k_0$ *and* $k_o = n_o k_0$ *be the wavenumber inside and outside the cavity, with* k_0 *the wavenumber in vacuum. Assume the incoming wave consists of* N *plane waves with frequency* $\omega = k_0 c$ *traveling in directions* $\theta_j \in [0, 2\pi], j = 1, 2, \ldots, N$*. Then the solution for the homogeneous Helmholtz equation, where the scattered field* ϕ_s *satisfies the Sommerfeld radiation condition* (5.15)*, is given by*

$$\begin{aligned} \phi(r,\theta) &= \begin{cases} \sum_{\nu=-\infty}^{\infty} C^i_\nu D^o_\nu J_\nu(k_i r) e^{i\nu\theta}, & \text{if } r < R \\ \phi_I(r,\theta) + \phi_s(r,\theta) & \text{if } r \geq R, \end{cases} \\ \phi_I(r,\theta) &= \sum_{\nu=-\infty}^{\infty} \left[D^o_\nu J_\nu(k_o r)\right] e^{i\nu\theta}, && \textit{incoming wave} \\ \phi_s(r,\theta) &= \sum_{\nu=-\infty}^{\infty} \left[C^o_\nu D^o_\nu H^{(1)}_\nu(k_o r)\right] e^{i\nu\theta}, && \textit{scattered wave} \end{aligned} \tag{5.23}$$

where D^o_ν *is given by* (5.20) *and* C^i_ν *and* C^o_ν *are given in* (5.22)*.*

From the expression for D^i_ν in (5.22) we can see that for small values of $J_\nu(k_i R)$, the coefficients inside the cavity might be large and thus ϕ might have large extrema in the oscillating behavior of the Bessel functions. This happens at a resonance. However, it might be that the numerator is small together with the denominator $J_\nu(k_i R)$. Then there is no resonance. However, the resonances we encounter in the circular cavity will take place for zeros of the Bessel functions, but not for all zeros there is a resonance. We will further investigate this when comparing with the numerical results.

We now show the analytical solution for some different frequencies in Figure 5.7. We set the refractive index $n_i = 5$ inside the cavity and $n_o = 1$ outside the cavity, to have a strong contrast and because of that, stronger resonance effects. The source consists of 100

random plane waves, as described by (5.19). The middle plot is close to a resonance, so the intensity of the wave is high inside the cavity.

Outside the cavity, the wave has irregular, non-circular shapes. This is caused by the fact that the source is random and thus is irregular shaped. Inside the cavity, especially at resonating behavior, the solution is almost symmetric around the center of the cavity.

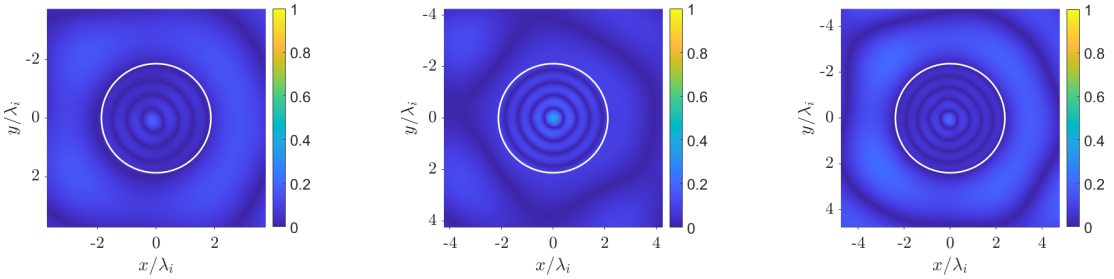

(a) $\omega = 1.10\times10^{13}$ rad/s (b) $\omega = 1.25\times10^{13}$ rad/s (c) $\omega = 1.50\times10^{13}$ rad/s

FIGURE 5.7: The absolute value of the analytical solution to Helmholtz equation, given in Theorem 1, plotted for $R = 64\mu m$, $n_i = 5$ and $n_o = 1$. The scaling factor $\lambda_i = \frac{2\pi}{n_i\omega}$ is the wavelength inside the cavity. The summation in (5.23) is taken from $-\nu_{\max}$ until $\nu_{\max}$, with $\nu_{\max} = 10$. The source consists of incident plane waves from 100 different random directions. The solution is shown for frequencies $\omega = 1.10\times10^{13}$, 1.25×10^{13} and 1.40×10^{13} rad/s. The resolution is $2\mu m^{-1}$. The white circle is the edge of the cavity.

5.2.3 Numerical results

To find a numerical solution with the method we again use BiCGSTAB, where we construct the preconditioned system using AnySim. Again we have $n_i = 5$ and $n_o = 1$. The resolution is $2\mu m^{-1}$ and the total square system has size $4R \times 4R$, with the radius of the cavity $R = 64\mu m$. For the absorbing boundaries, a boundary width of $512\mu m$ is put on all sides.

It was chosen to use plane waves from random directions, with random amplitude and with random phase as the random source ψ. These are the same plane waves as used to find the analytical solutions, described in (5.19). When instead using the simpler white noise, as we did with the 1D Fabry-Perot resonator, there was square behaviour in what should be a cylindrically symmetric system. This is likely due to the fact that with white noise, a large part of the source is contained in the corners of the square system, removing the symmetry around the origin. When using plane waves from random directions, this effect was mostly removed. Using plane waves also has the advantage that the comparison with the analytical solution is much more appropriate, because the same source is used. It also represents better what would happen in a physical system, where the cavity would likely be excited with plane waves.

The achieved solutions for a few frequencies are plotted in Figure 5.8.

We see that the behavior inside the cavity is similar between the analytical and numerical solution, especially for the resonating frequency. The resonating behaviour at $\omega = 1.25\times10^{13}$ is clearly visible in both cases. Outside the cavity, however, the solution is somewhat different. The effects of these differences on the behaviour inside the cavity, especially at the resonance, seems to be minimal.

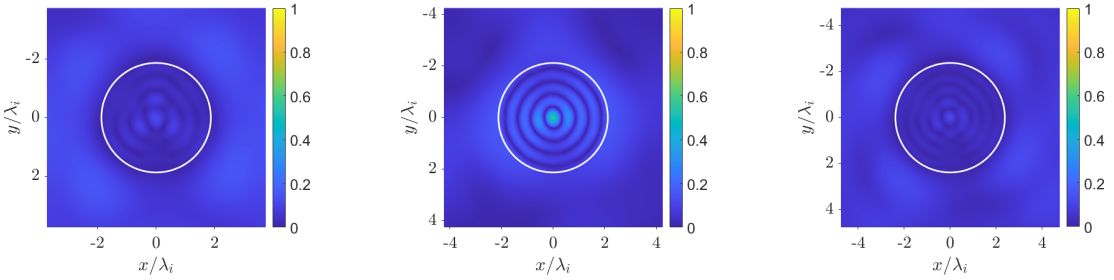

(a) $\omega = 1.10{\times}10^{13}$ rad/s (b) $\omega = 1.25{\times}10^{13}$ rad/s (c) $\omega = 1.50{\times}10^{13}$ rad/s

FIGURE 5.8: The absolute value of the solution to Helmholtz equation, simulated using AnySim with BiCGSTAB, plotted for $R = 64\mu m$, $n_i = 5$ and $n_o = 1$. The scaling factor $\lambda_i = \frac{2\pi}{n_i \omega}$ is the wavelength inside the cavity. The source consists of incident plane waves from 100 different random directions. The solution is shown for frequencies $\omega = 1.10{\times}10^{13}$, $1.25{\times}10^{13}$ and $1.40{\times}10^{13}$ rad/s. The resolution is $2\mu m^{-1}$. The white circle is the edge of the cavity.

We can now introduce the norm function for the circular cavity in two dimensions which can be used to determine the resonating frequencies. We can use the same function for both the analytical solution and the numerical solution.

$$f(\omega) = \frac{1}{\|\phi\|_{r<R}}, \tag{5.24}$$

where $\|\cdot\|_{r<R}$ denotes the L^2-norm over the cavity $r < R$ for square-integrable functions:

$$\|\phi\|_{r<R} = \iint_{r<R} |\phi(r,\theta)|^2 dA$$

For the analytical solution we can rewrite this and use the orthogonality of complex exponentials around a cylinder, since $\int_{\theta=0}^{\theta=2\pi} e^{i\nu\theta} d\theta = 0$ for $\nu \in \mathbb{Z}\backslash\{0\}$ and 2π otherwise.

$$\begin{aligned}
&\iint_{r<R} |\phi(r,\theta)|^2 dA \\
&= \int_{r=0}^{R} \int_{\theta=0}^{\theta=2\pi} \sum_{\nu=-\infty}^{\infty} C_\nu^i D_\nu^o J_\nu(k_i r) e^{i\nu\theta} \sum_{\nu'=-\infty}^{\infty} C_{\nu'}^{i*} D_{\nu'}^{o*} J_{\nu'}^*(k_i r) e^{-i\nu'\theta} d\theta r dr \\
&= \int_{r=0}^{R} \int_{\theta=0}^{\theta=2\pi} \sum_{\nu=-\infty}^{\infty} \sum_{\nu'=-\infty}^{\infty} C_\nu^i D_\nu^o J_\nu(k_i r) C_{\nu'}^{i*} D_{\nu'}^{o*} J_{\nu'}^*(k_i r) e^{i(\nu-\nu')\theta} d\theta r dr \\
&= \int_{r=0}^{R} \sum_{\nu=-\infty}^{\infty} |C_\nu^i|^2 |D_\nu^o|^2 |J_\nu(k_i r)|^2 2\pi r dr \\
&= 2\pi \sum_{\nu=-\infty}^{\infty} |C_\nu^i|^2 |D_\nu^o|^2 \int_{r=0}^{R} |J_\nu(k_i r)|^2 r dr,
\end{aligned}$$

where the orthogonality is used in the fourth line. We see that the norm is largely dependent on the coupling coefficient C_ν^i. An analytical solution to the integral of the Bessel function is stated in [18], but we choose to evaluate the norm numerically for simplicity.

For a numerical solution that is a matrix with the wave intensity at each grid point, this norm is discretized by taking the norm of the matrix, while only including the part of the matrix that corresponds to the cavity.

The function $f(\omega)$ we get from the analytical solution can be compared to the $f(\omega)$ we get using the numerical method. We especially expect the minima of both functions to be similar, since the resonant modes should be excited in the numerical solution as well as the analytical solution.

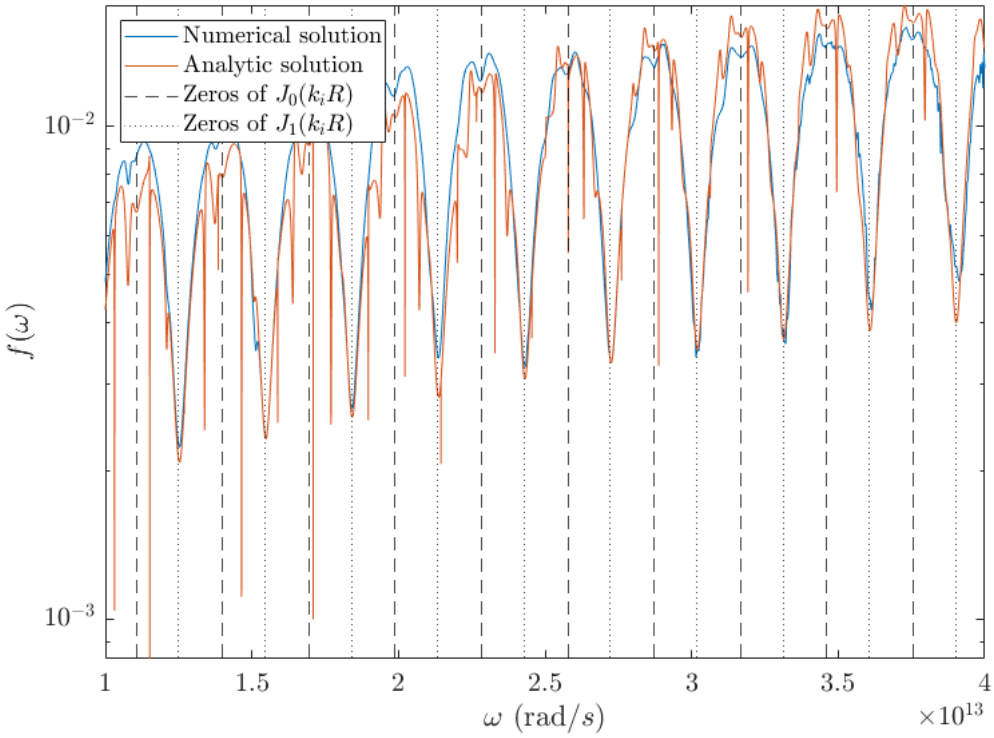

FIGURE 5.9: The inverse norm function $f(\omega)$ normalized for both the analytical solution and the solution from the numerical method using AnySim with BiCGSTAB. $R = 64\mu m$, $n_i = 5$ and $n_o = 1$. The resolution for the numerical method is $2\mu m^{-1}$. The sources are plane waves from 100 different random directions, which are the same for the analytical and numerical solution. Also plotted are vertical lines at the ω for which $J_{0,1}(k_iR) = J_{0,1}(\frac{n_i\omega}{c}R) = 0$.

In Figure 5.9, the function $f(\omega)$ is plotted for both the analytical and numerical solution. Also the frequencies for which the Bessel functions with orders 0 and 1 have a zero are plotted, as vertical lines. We only look at the real zeros of the Bessel function, as we look to find real frequencies.

We directly notice that $f(\omega)$ is very similar for both solutions. The wide minima are located at approximately the same frequencies ω.

For the analytic solution, $f(\omega)$ shows some irregularities, namely very sharp peaks downward. These peaks are caused by numerical errors at removable singularities in the coupling coefficients of the analytical solution.

To give an example of this, we look at the peak that exists at $\omega_0 = 2.5793\times10^{13}$ rad/s. This value coincides with a zero of $J_0(k_iR)$. However, in this case, $J_0(k_oR)$ also has a zero

for this wavelength. To study the behavior of the expressions of C_0^o and C_0^i, we take the limit as $\omega \to \omega_0$. We first approach this limit in the expression for E_0^o in (5.22):

$$\begin{aligned}
\lim_{\omega\to\omega_0} C_0^o &= \lim_{\omega\to\omega_0} \frac{\frac{J_0(k_oR)}{J_0(k_iR)} - \frac{k_oJ_0'(k_oR)}{k_iJ_0'(k_iR)}}{\frac{k_oH_0^{(1)\prime}(k_oR)}{nJ_0'(k_iR)} - \frac{H_0^{(1)}(k_oR)}{J_0(k_iR)}} \\
&= \lim_{\omega\to\omega_0} \frac{J_0(k_oR) - J_0(k_iR)\frac{k_oJ_0'(k_oR)}{k_iJ_0'(k_iR)}}{J_0(k_iR)\frac{k_oH_0^{(1)\prime}(k_oR)}{nJ_0'(k_iR)} - J_0(k_oR) - iY_0(k_oR)} \\
&= \frac{0-0}{0-0-iY_0(k_oR)} = 0,
\end{aligned}$$

where in the last line we used that $Y_0(k_oR) \neq 0$, since the zeros of the Bessel function of the first and second kind are distinct (see e.g. [1]). We also used the definition of $H_0^{(1)\prime}(k_oR)$, given in (5.11).

We can approach the same limit for C_0^i in the expression for D_0^i in (5.22):

$$\begin{aligned}
\lim_{\omega\to\omega_0} C_0^i &= \lim_{\omega\to\omega_0} \frac{J_0(k_oR) + C_0^oH_0^{(1)}(k_oR)}{J_0(k_iR)} \\
&= \lim_{\omega\to\omega_0} \frac{J_0(k_oR) + \frac{J_0(k_oR) - J_0(k_iR)\frac{k_oJ_0'(k_oR)}{k_iJ_0'(k_iR)}}{J_0(k_iR)\frac{k_oH_0^{(1)\prime}(k_oR)}{nJ_0'(k_iR)} - J_0(k_oR) - iY_0(k_oR)} H_0^{(1)}(k_oR)}{J_0(k_iR)} \\
&= \lim_{\omega\to\omega_0} \frac{J_0(k_oR)}{J_0(k_iR)} + \frac{J_0(k_oR)^2 + iJ_0(k_oR)Y_0(k_oR)}{J_0(k_iR)\left(J_0(k_iR)\frac{k_oH_0^{(1)\prime}(k_oR)}{nJ_0'(k_iR)} - J_0(k_oR) - iY_0(k_oR)\right)} \\
&\quad - \frac{\frac{k_oJ_0'(k_oR)}{k_iJ_0'(k_iR)}(J_0(k_oR) + iY_0(k_oR))}{J_0(k_iR)\frac{k_oH_0^{(1)\prime}(k_oR)}{nJ_0'(k_iR)} - J_0(k_oR) - iY_0(k_oR)} \\
&= \frac{J_0'(k_oR)}{J_0'(k_iR)}\left(1 + \frac{iY_0(k_oR)}{-iY_0(k_oR)}\right) - \frac{k_oJ_0'(k_oR)}{k_iJ_0'(k_iR)}\frac{iY_0(k_oR)}{-iY_0(k_oR)} \\
&= \frac{J_0'(k_oR)}{J_0'(k_iR)}\frac{k_o}{k_i}.
\end{aligned} \tag{5.25}$$

We again used that $Y_0(k_oR) \neq 0$, and also used the fact from [1] that all the zeros of the Bessel function are simple, so the value of the derivative J_0' at the zeros of the Bessel function is non-zero. Therefore we could apply l'Hôpital in the fourth line.

Thus, we have shown that the singularity at $\omega_0 = 2.5793\times10^{13}$ rad/s is removable, since the limit of $\omega \to \omega_0$ exists (see e.g. [17]). Similar singularities happen at other sharp peaks in Figure 5.9, where the order of the Bessel function ν for which the singularity exists might be different.

Because the Bessel functions are evaluated numerically, the division in the coupling coefficients is not exact and the result is that the numerical values for $C_\nu^o = 0$ and $C_\nu^i = 0$ become very large at some of those singularities, while they are not analytically. That results in the fact that $f(\omega)$ is very small, while there is no real resonance behaviour. Therefore we decide to ignore the very sharp peaks when the analytical results are compared with the numerical results.

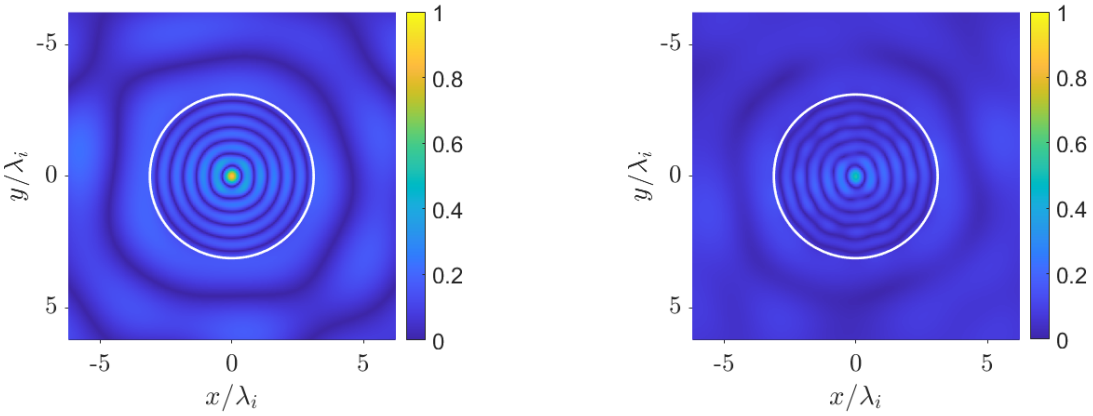

(a) (b)

FIGURE 5.10: The absolute value of the solution to Helmholtz equation, (a) analytical and (b) numerical. The solution is shown for the resonant frequency $\omega = 1.8316\times10^{13}$ rad/s, which was found with the numerical solution. $R = 64\mu m$, $n_i = 5$ and $n_o = 1$. The scaling factor $\lambda_i = \frac{2\pi}{n_i\omega}$ is the wavelength inside the cavity. The sources are plane waves from 100 different random directions, which are the same for the analytical and numerical solution. The resolution is $2\mu m^{-1}$. The white circle is the edge of the cavity.

In Figure 5.9, we see that there is a smooth minimum around $\omega = 1.25\times10^{13}$ rad/s, which points towards resonating behaviour. We saw this already in Figures 5.7b and 5.8b.

Now the method using AnySim can be used to further minimize $f(\omega)$, using Matlab's `fminsearch` function. When we take $\omega = 1.80\times10^{13}$ rad/s as an initial guess, we reach the minimum at $\omega = 1.8316 \pm 0.0001\times10^{13}$ rad/s, for which the analytical and numerical solutions are plotted in Figure 5.10.

We can also minimize $f(\omega)$ by using the analytic solution. With the same initial guess we get then the minimum at $\omega = 1.8396 \pm 0.0001\times10^{13}$ rad/s. Again we plot the solution, in Figure 5.11.

We see that the value found for ω with the analytical solution (1.8402×10^{13} rad/s) is more exact. The resonance is slightly stronger here than for $\omega = 1.8316\times10^{13}$ rad/s, as the maximal intensity in the rings is slightly larger, looking at the analytical solution. This is better visible in Figure 5.12. In this figure, the value of the analytical solution on the positive x-axis is given for both frequencies. The intensity is larger for the analytically found frequency.

When referring back to Figure 5.9, we see that the analytical and numerical solution show mimina at or very close to the zeros of the Bessel function of first order. This is as expected from the expressions of the coefficients in (5.22), where at a zero of the Bessel function, we have a pole in C^i_ν (except for the cases where the singularity is removable, as was discussed before). At such a pole, the coupling coefficient C^i_ν is very large and thus the norm over the cavity is large.

The zeros of the Bessel function of order 0 are not visible much in the minima of $f(\omega)$. Both the analytical and numerical solution show a small drop for most zeros. Some of the zeros are removable singularities, as we argued before, so are not a resonance. Apparently, for the other zeros, the resonance is not strong. This might be explained by the shape of

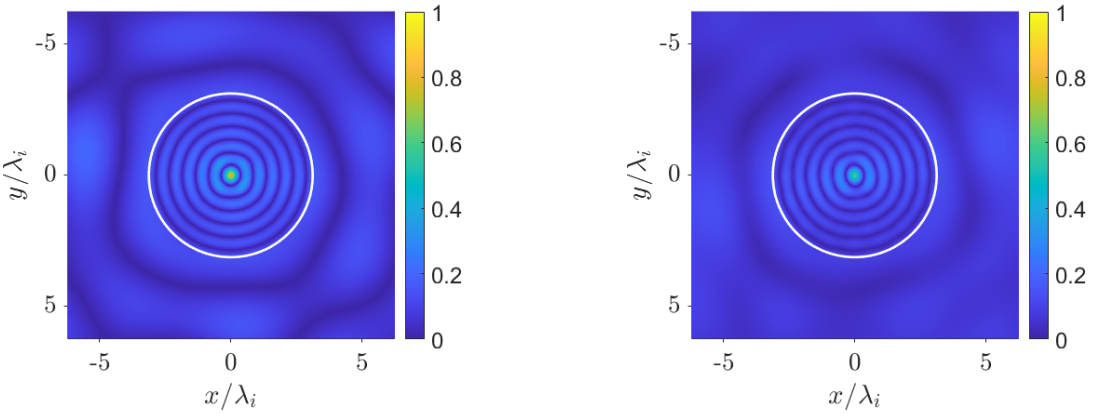

FIGURE 5.11: The absolute value of the solution to Helmholtz equation, (a) analytical and (b) numerical. The solution is shown for the resonant frequency $\omega = 1.8396{\times}10^{13}$ rad/s, which was found with the analytic solution. $R = 64\mu m$, $n_i = 5$ and $n_o = 1$. The scaling factor $\lambda_i = \frac{2\pi}{n_i \omega}$ is the wavelength inside the cavity. The sources are plane waves from 100 different random directions, which are the same for the analytical and numerical solution. The resolution is $2\mu m^{-1}$. The white circle is the edge of the cavity.

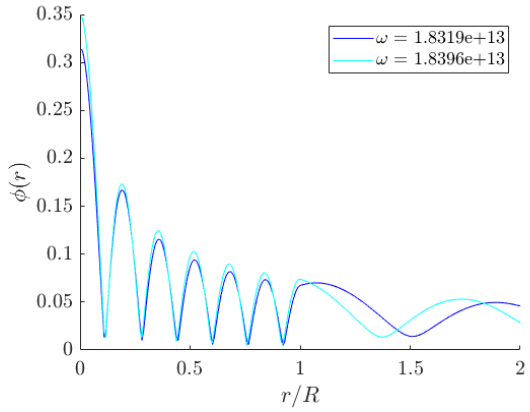

FIGURE 5.12: The absolute value of the analytical solution to Helmholtz equation as a function of r, for $\omega = 1.8316{\times}10^{13}$ rad/s and $\omega = 1.8402{\times}10^{13}$ rad/s. $R = 64\mu m$, $n_i = 5$ and $n_o = 1$. The sources are plane waves from 100 different random directions. The resolution is $2\mu m^{-1}$.

Initial guess based on Figure 5.9 (rad/s)	$\text{argmin}_\omega f_{\text{An.}}(\omega)$ (rad/s) ($\pm 0.001 \times 10^{13}$ rad/s)	rel. err.	$\text{argmin}_\omega f_{\text{Num.}}(\omega)$ (rad/s) ($\pm 0.001 \times 10^{13}$ rad/s)	rel. err.	ω s.t. $J_1(\frac{n_i \omega}{c} R) = 0$ (rad/s)
1.26×10^{13}	1.249×10^{13}	0.3×10^{-4}	1.251×10^{13}	0.002	1.249×10^{13}
1.54×10^{13}	1.544×10^{13}	1×10^{-4}	1.548×10^{13}	0.002	1.544×10^{13}
1.84×10^{13}	1.840×10^{13}	1×10^{-4}	1.832×10^{13}	0.004	1.839×10^{13}
2.14×10^{13}	2.134×10^{13}	0.9×10^{-4}	2.137×10^{13}	0.002	2.134×10^{13}
2.42×10^{13}	2.429×10^{13}	1×10^{-4}	2.435×10^{13}	0.003	2.428×10^{13}
2.72×10^{13}	2.723×10^{13}	1×10^{-4}	2.718×10^{13}	0.002	2.723×10^{13}
3.02×10^{13}	3.018×10^{13}	1×10^{-4}	3.019×10^{13}	3×10^{-4}	3.018×10^{13}
3.31×10^{13}	3.313×10^{13}	1×10^{-4}	3.318×10^{13}	0.002	3.312×10^{13}
3.60×10^{13}	3.607×10^{13}	1×10^{-4}	3.614×10^{13}	0.002	3.607×10^{13}
3.90×10^{13}	3.902×10^{13}	1×10^{-4}	3.908×10^{13}	0.002	3.902×10^{13}

TABLE 2: ω at which there is a resonance. Column 1 is the initial guess that is used for the minimizer function `fminsearch` by Matlab (see [6]) that is used to find the values in column 2 and 4. In those columns the ω are given which are the minima of $f(\omega)$ from the analytical and numerical solution, respectively. $f(\omega)$ is given by (5.24). The last column then gives the ω such that the Bessel function of order 1 has a zero that is corresponding to the ω presented in columns 2 and 4. Column 3 and 5 give the relative error of column 2 and 4 with respect to the zeros of the Bessel function in the last column.

the Bessel function. The Bessel function of order 0 is equal to 1 at 0, but decreases quickly and the next extrema have a much smaller amplitude. That means that at those resonances, the field is only large very close to the origin and is not strong further outwards. Therefore, the resonance is not strong at those zeros.

We now compare the performance of the method using AnySim with the zeros found by the analytic solution, both using $f(\omega)$ and the zeros of the Bessel function in Table 2. In the table, only the zeros of the Bessel function of order 1 are used, since at those frequencies the numerical method is able to find a minimum of $f(\omega)$ and a resonant mode. In the table, it is visible that $f_{\text{An.}}(\omega)$ has its minima very close to the zeros of the Bessel function, which is as expected from the analytic expression for D^i_ν in 5.22. The result is very precise and in the order of the tolerance of the minimizer.

For the values found numerically using the method based on AnySim, the relative error is larger. However, it is still small, with a maximum of 0.4% for the 10 cases in the table.

In conclusion, the method using AnySim is able to accurately find the resonating frequencies for strong, smooth resonances of a dielectric circular cavity in two dimensions. Those resonances correspond to zeros of the Bessel function of order 1. The solutions at the resonating frequencies are very similar to the analytic solutions. Smaller resonances are often not excited in the numerical solution and are therefore not located by the method. These resonances are also barely visible when using the analytical solution, however, and thus are not strong resonances and of less importance for applications.

5.3 Dielectric circular cavity with edge distortion

To illustrate a more practical use of our method, we consider the same dielectric circular cavity as before, but now with small parts taken out of the circle, which remove the cylindrical symmetry. These parts taken out of the circle could represent production defects of a perfectly circular cavity. If small changes in the edges have a large effect on the resonating frequencies, a nanoparticle of that shape will likely not be useful in practice, as production defects, which will always exist, will drastically change the behavior of the

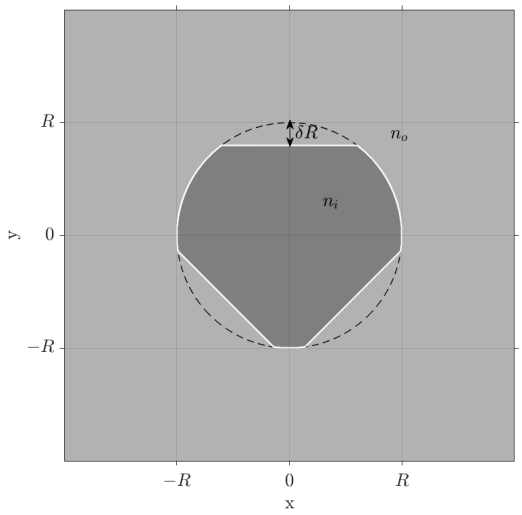

FIGURE 5.13: Setup for the dielectric circular cavity with edge distortion. The size of the defects δR is exaggerated in the figure to illustrate what is done. The refractive index is equal to n_i inside and n_o outside.

nanoparticle.

The shape was made by cutting of a part of the circle on 3 sides. We call the size of the defects δR. We will vary this size to study how much the eigenmodes change with respect to the perfect situation, which was studied in Section 5.2. An illustration of the setup is given in Figure 5.13.

With the same parameters as used with the perfect circular cavity, we evaluate $f(\omega)$ for different values of δR. The results are visible in Figure 5.14.

In this figure we see that the minima of $f(\omega)$ move to somewhat higher frequencies if the deformations become larger. Some of the reflections at the boundary are now closer to the center, so we would expect that the resonating wavelength is smaller, so the minima indeed have higher frequency. We see that for $\delta R = 2.5\mu m$, the minimum is still close to the minimum of a perfect circle. For higher deformations, the modes are at a significantly different frequency and show less resonating behavior.

We also notice that the peaks get slightly higher and wider for larger δR. Because the circular symmetry is removed, the resonating behavior is weaker. What is interesting, is that the peak is lower for δR =0.5 and 2.5 μm. Apparently, these small deformations help to excite the resonant modes. The deformations might produce some irregular shapes in the wave function that are closely related to the resonant modes.

We now show the solutions at the minimum of $f(\omega)$ at $\omega = 1.548 \times 10^{13}$ rad/s for the perfect circle and deformations of δR =2.5 and 5.0 μm at the same frequency. For $\delta R = 5.0\mu m$ we also plot the solution at its resonance at $\omega = 1.584 \times 10^{13}$ in Figure 5.15. The minima were again found using `fminsearch` with the initial guesses chosen based on Figure 5.14.

In Figures 5.15a and 5.15b, we see that the resonant mode of the deformed circle with $\delta R = 2.5\mu m$, is at the same frequency, and very similarly shaped, as the mode of the perfect circle with no deformation. There are some irregularities in the solution, but the main circular shape is still present.

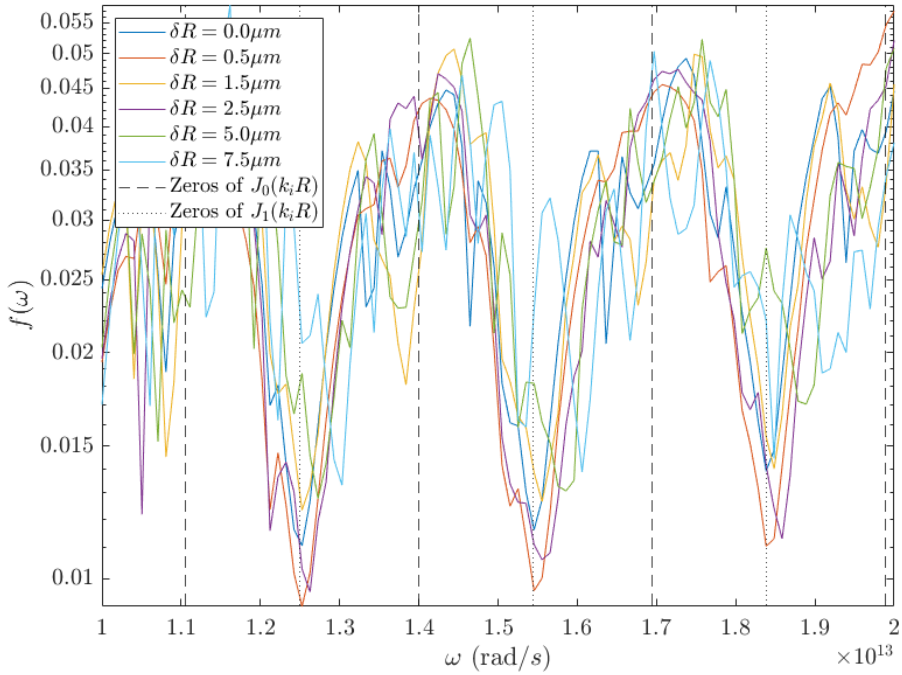

FIGURE 5.14: The inverse norm function $f(\omega)$, normalized for the area of the cavity, for a circular cavity with a part with size δR cut off at 3 sides. The function is evaluated for different values of δR. $R = 64\mu m$, $n_i = 5$ and $n_o = 1$. The resolution for the numerical method is $2\mu m^{-1}$. The sources are plane waves from 100 different random directions. Also plotted are vertical lines at the ω for which $J_{0,1}(k_i R) = J_{0,1}(\frac{n_i \omega}{c} R) = 0$.

However, for $\delta R = 5.0\mu m$, we see in Figure 5.15c that the solution does not show any resonant behavior for $\omega = 1.548 \times 10^{13}$ rad/s, which is a resonant frequency for the perfect circle. Moreover, for $\omega = 1.584 \times 10^{13}$, there is a resonant mode for the deformed shape with $\delta R = 5.0\mu m$, however it is very different from the circular shaped mode of a perfect circle. We thus see that the resonating behavior has changed drastically from adding the deformations.

We can thus conclude that deformations smaller than $2.5\mu m$ will have modes that are very similar to the modes of a perfect circle. With a radius of $R = 64\mu m$, this is around 4% of the radius. The resonating behavior of the circle is thus not very sensitive to production defects. For larger defects, however, the resonance of the modes changes and the cavity behaves very different than a perfect circle.

With this example we have shown that the method that was introduced has practical uses and can efficiently be used to approximate eigenfrequencies and the corresponding wave function for irregular shaped cavities, for which an analytical solution does not exist.

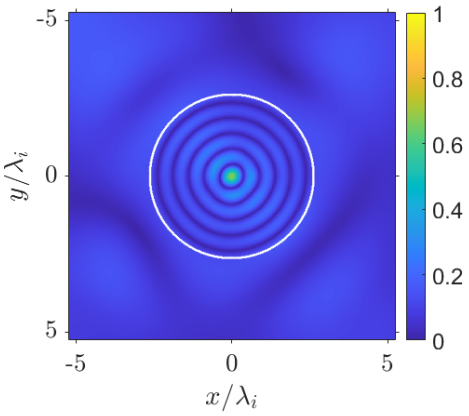

(a) $\delta R = 0$,
$\omega = 1.548{\times}10^{13}$ rad/s

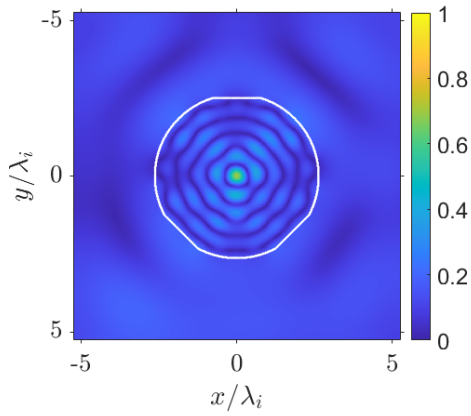

(b) $\delta R = 2.5\mu m$,
$\omega = 1.548{\times}10^{13}$ rad/s

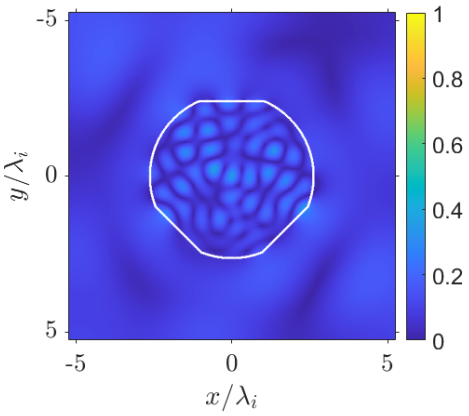

(c) $\delta R = 5.0\mu m$,
$\omega = 1.548{\times}10^{13}$ rad/s

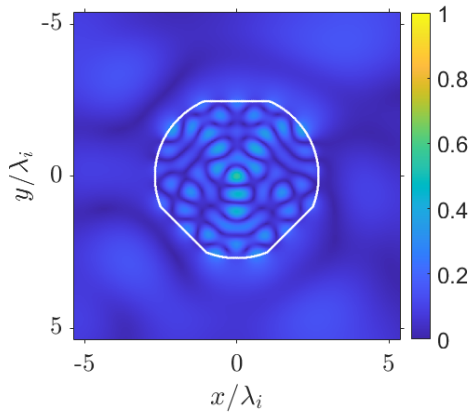

(d) $\delta R = 5.0\mu m$,
$\omega = 1.584{\times}10^{13}$ rad/s

FIGURE 5.15: The absolute value of the solution to Helmholtz equation, simulated using AnySim with BiCGSTAB, plotted for $R = 64\mu m$, $n_i = 5$ and $n_o = 1$. The solution is shown for a perfect and a slightly deformed circle. The scaling factor $\lambda_i = \frac{2\pi}{n_i \omega}$ is the wavelength inside the cavity. The source consists of incident plane waves from 100 different random directions. The resolution is $2\mu m^{-1}$. The white shape is the edge of the cavity.

6 Discussion and Recommendations

In the different problems studied, we have seen that in many cases, the introduced method is able to find accurate estimates of the eigenfrequencies of a system and produce a mode that is very similar to the analytical solution. However, in some cases, for low frequency and asymmetric modes, we saw that the method struggles to find the resonant modes. These shortcomings are likely due to the way the system is excited with random waves. To improve on this, it might be tried to use other sources to excite the system. A plane wave, instead of white noise, might increase the performance in the one-dimensional case.

We saw that in the two-dimensional system, where plane waves resulted in a more accurate solution of the system, the ability to excite modes was also increased with respect

to white noise. Using plane waves is also more realistic when looking from a physical perspective. A physical cavity will always be excited with waves with a certain frequency and can not have white noise as its source.

To further improve performance by tuning the source, one might use other waveshapes in two or three dimensions, such as radial waves. These might have an even better ability to excite the resonant modes.

In the current implementation, it is not possible to use complex frequencies with negative imaginary part, which are needed in the case of quasi-normal modes. This is because the Helmholtz equation is not accretive in the case of wavenumber with negative imaginary part. We have seen that the minima of $f(\omega)$ with real ω are at the same position as the real part of the quasi-normal mode frequencies. Since we can only excite a physical system with a real frequency, the fact that we can only find real resonating frequencies is not unacceptable. However, for finding the shape of the eigenmodes, it is needed to handle complex frequencies. Currently, the approximations of the modes is not exact, since we are not exactly at the eigenfrequency. Therefore, other modes are present in the approximation of the eigenmodes.

The system can be altered to make it accretive. A method to do this is described in [20]. Doing this doubles the size of the system and thus increases the computation time drastically. However, when the aim is to find the exact modes, this will be a method to increase the accuracy.

It was found that BiCGSTAB performs well, when compared to GMRES and the Richardson iteration, close to resonances. The preconditioner method is not proven to be effective with the BiCGSTAB method, however. The preconditioning is needed for convergence; the BiCGSTAB algorithm does not converge when solving the original unpreconditioned system. Convergence for BiCGSTAB is difficult to prove (see [21]), but it is useful to study the behavior of BiCGSTAB in combination with the preconditioner, such that it can be understood why it works well close to resonances.

To solve the linear system in our experiments, both the resolution of the grid and the size of the absorbing boundaries was set constant. However, to increase efficiency, these parameters could be made dependent on the wavelength and frequency. The resolution can be less for longer wavelengths, as generally the needed resolution is a constant number of grid points per wavelength. This decreases the time needed for computations by the BiCGSTAB algorithm.

The size of the absorbing boundaries can be smaller for shorter wavelengths, because the absorbing boundary has to have the length of around 10 wavelengths. Also other absorbing boundary methods can be used that need less boundary width and therefore are more computationally efficient.

The minimization of $f(\omega)$ is currently done using the function `fminsearch` of Matlab. This function performs well and, in the examples studied, mostly finds the minimum with a precision of $\frac{\Delta\omega}{\omega} = 1 \times 10^{-4}\text{rad}/s$ in around 10 iterations and 25 function evaluations. Other minimalization methods that are more specific for the kind of function that $f(\omega)$ is, can have a better performance. The minima of $f(\omega)$ are namely sharply shaped, with the absolute value of the slope increasing until very close to the minimum.

When expanding towards complex frequencies, definitely another minimization method has to be chosen. `fminsearch` namely only works for real input variables. For example,

steepest descent can be used. However, since the hypothesis is that the minima on the real axis correspond to the real part of the minima in the complex plane, one might also choose to do the minimization separately for real and imaginary part.

Currently, the initial guess for the minimization function was chosen based on a line search, where by hand the minima were estimated based on a graph. One might construct an algorithm in which the initial guesses are chosen by the algorithm instead of doing that by hand.

Also, the non-convergence of the Richardson iteration at eigenfrequencies can maybe be used. It was observed and argued that the residual of the Richardson iteration grows indefinitely when the system is solved at an eigenfrequency. This makes the iteration very inefficient close to eigenfrequencies, but in other cases it is quicker than for example BiCGSTAB, since the iterations are much simpler. One might use the Richardson iteration method to do the first line search method and assume that the minimum lies in a range where the Richardson iteration converges slowly. The Richardson iteration can then be cut off when it is observed that the convergence is slow, such that the iteration method does not have to be completed. When using the minimizer method, BiCGSTAB or something similar has to be used to compute a solution to the system close to a resonance.

7 Conclusion

A method was constructed that locates the eigenfrequencies ω of an operator $A(\omega)$ and can find an approximation of the eigenmodes or quasi-normal modes. This method excites the resonating eigenmodes with a random source ψ and then solves the system $A(\omega)\phi = \psi$. This system is solved with the help of a universal preconditioner. When the preconditioned system is constructed, the system can be solved using the BiCGSTAB algorithm and based on the norm of this solution, the eigenfrequencies can be determined. The found solution also is a good approximation of the eigenmode.

The method was validated for the case of the Helmholtz equation for cavities in one and two dimensions. From comparison with analytical solutions, it was found that the method finds the eigenfrequencies accurately in most cases. Also an accurate estimate of the eigenfunction is produced by the method. For low-frequency antisymmetric modes, the method did not locate the eigenmodes, however.

8 References

[1] Milton Abramowitz and Irene A. Stegun. *Handbook of Mathematical Functions: With Formulas, Graphs, and Mathematical Tables*. Courier Corporation, Jan. 1965. ISBN: 978-0-486-61272-0.

[2] George B. Arfken and Hans-Jurgen Weber. *Mathematical methods for physicists*. 6th ed. Chapter 11 about Bessel functions. Boston: Elsevier, 2005. ISBN: 978-0-12-059876-2.

[3] W. E. Arnoldi. "The principle of minimized iterations in the solution of the matrix eigenvalue problem". In: *Quarterly of Applied Mathematics* 9.1 (1951), pp. 17–29. ISSN: 0033-569X, 1552-4485. DOI: 10.1090/qam/42792.

[4] H. Cheng et al. "Fast, accurate integral equation methods for the analysis of photonic crystal fibers I: Theory". In: *Optics Express* 12.16 (Aug. 2004), pp. 3791–3805. ISSN: 1094-4087. DOI: 10.1364/opex.12.003791.

[5] David Colton and Rainer Kress. *Inverse Acoustic and Electromagnetic Scattering Theory*. Springer Science & Business Media, Oct. 2012. ISBN: 978-1-4614-4942-3.

[6] *Find minimum of unconstrained multivariable function using derivative-free method - MATLAB fminsearch - MathWorks Benelux*. URL: https://nl.mathworks.com/help/matlab/ref/fminsearch.html (visited on 06/09/2023).

[7] David J. Griffiths. *Introduction to Electrodynamics*. Pearson Education, Jan. 2014. ISBN: 978-0-321-97210-1.

[8] Isaac Harari. "A survey of finite element methods for time-harmonic acoustics". In: *Computer Methods in Applied Mechanics and Engineering* 195 (Feb. 2006), pp. 1594–1607. DOI: 10.1016/j.cma.2005.05.030.

[9] Mathew Kallumadil et al. "Corrigendum to "Suitability of commercial colloids for magnetic hyperthermia" [J. Magn. Magn. Mater. 321 (2009) 1509–1513]". In: *Journal of Magnetism and Magnetic Materials*. Current Perspectives: Magnetocaloric Materials 321.21 (Nov. 2009), pp. 3650–3651. ISSN: 0304-8853. DOI: 10.1016/j.jmmm.2009.06.069.

[10] Bruce R. Kusse and Erik A. Westwig. *Mathematical Physics: Applied Mathematics for Scientists and Engineers*. Wiley, Mar. 2006. ISBN: 978-3-527-40672-2.

[11] Philippe Lalanne et al. "Light Interaction with Photonic and Plasmonic Resonances". In: *Laser & Photonics Reviews* 12.5 (2018), p. 1700113. ISSN: 1863-8899. DOI: 10.1002/lpor.201700113.

[12] P. T. Leung, S. Y. Liu, and K. Young. "Completeness and orthogonality of quasinormal modes in leaky optical cavities". In: *Physical Review A* 49.4 (Apr. 1994). Publisher: American Physical Society, pp. 3057–3067. DOI: 10.1103/PhysRevA.49.3057.

[13] Albert H. Nuttal. "Some windows with very good sidelobe behavior". In: *IEEE Transactions on Acoustics, Speech, and Signal Processing* 29.1 (Feb. 1981). Conference Name: IEEE Transactions on Acoustics, Speech, and Signal Processing, pp. 84–91. ISSN: 0096-3518. DOI: 10.1109/TASSP.1981.1163506.

[14] Gerwin Osnabrugge, Saroch Leedumrongwatthanakun, and Ivo Vellekoop. "A convergent Born series for solving the inhomogeneous Helmholtz equation in arbitrarily large media". In: *Journal of Computational Physics* 322 (Jan. 2016). DOI: 10.1016/j.jcp.2016.06.034.

[15] Frank L. Pedrotti, Leno M. Pedrotti, and Leno S. Pedrotti. *Introduction to Optics*. Cambridge University Press, Dec. 2017. ISBN: 978-1-108-42826-2.

[16] Youcef Saad and Martin H. Schultz. "GMRES: A Generalized Minimal Residual Algorithm for Solving Nonsymmetric Linear Systems". In: *SIAM Journal on Scientific and Statistical Computing* 7.3 (July 1986). Publisher: Society for Industrial and Applied Mathematics, pp. 856–869. ISSN: 0196-5204. DOI: 10.1137/0907058.

[17] E. B. Saff and Arthur David Snider. *Fundamentals of Complex Analysis with Applications to Engineering and Science*. Prentice Hall, 2003. ISBN: 978-0-13-907874-3.

[18] Renato Spigler. "Sulle radici dell'equazione: A Jv(x)+BxJv'(x)". In: *Atti Sem. Mat. Fis. Univ. Modena* 24 (Jan. 1975), pp. 399–419.

[19] Orazio Svelto. *Principles of Lasers*. Springer Science & Business Media, Mar. 2010. ISBN: 978-1-4419-1302-9.

[20] Tom Vettenburg and Ivo M. Vellekoop. "A universal preconditioner for linear systems". In: (July 2022). DOI: 10.48550/arXiv.2207.14222.

[21] H. A. van der Vorst. "Bi-CGSTAB: A Fast and Smoothly Converging Variant of Bi-CG for the Solution of Nonsymmetric Linear Systems". In: *SIAM Journal on Scientific and Statistical Computing* 13.2 (Mar. 1992). Publisher: Society for Industrial and Applied Mathematics, pp. 631–644. ISSN: 0196-5204. DOI: 10.1137/0913035. (Visited on 06/20/2023).

[22] Muhammad Zubair, M. Mughal, and Q. Naqvi. "The wave equation and general plane wave solutions in fractional space". In: *Progress In Electromagnetics Research Letters* 19 (Jan. 2011), pp. 137–146. DOI: 10.2528/PIERL10102103.